Lipid biomarker and stable isotopic profiles through Early-Middle Ordovician carbonates from Spitsbergen, Norway

Carina Lee[a,b*], Gordon D. Love[b], Melanie J. Hopkins[c], Björn Kröger[d], Franziska Franeck[e], and Seth Finnegan[a]

[a]*Department of Integrative Biology, University of California, Berkeley, 3040 Valley Life Sciences Building #3140, Berkeley California, USA 94720 (carina.lee@berkeley.edu, sethf@berkeley.edu)*

[b]*Department of Earth Sciences, University of California, Riverside, 900 University Avenue, Riverside California, USA 92521(gordon.love@ucr.edu)*

[c]*Division of Paleontology, American Museum of Natural History, Central Park West at 79th Street, New York City, New York, USA 10034 (mhopkins@amnh.org)*

[d]*Finnish Museum of Natural History, PO Box 44, Fi-00014 University of Helsinki, Helsinki, Finland (bjorn.kroger@helsinki.fi)*

[e]*Centre for Ecological and Evolutionary Synthesis, University of Oslo, Postboks 1172, Blindern 0318 Oslo, Norway (franziska.franeck@nhm.uio.no)*

**corresponding author*

ABSTRACT

One of the most dramatic episodes of sustained diversification of marine ecosystems in Earth history took place during the Early to Middle Ordovician Period. Changes in climate, oceanographic conditions, and trophic structure are hypothesised to have been major drivers of these biotic events, but relatively little is known about the composition and stability of marine microbial communities controlling biogeochemical cycles at the base of the food chain. This study examines well-preserved, carbonate-rich strata spanning the Tremadocian through Upper Dapingian stages from the Oslobreen Group in Spitsbergen, Norway. Abundant bacterial lipid markers (elevated hopane/sterane ratios, average = 4.8; maximum of 13.1), detection of Chlorobi markers in organic-rich strata, and bulk nitrogen isotopes ($\delta^{15}N_{total}$) averaging 0 to -1‰ for the

open marine facies, suggest episodes of water column redox-stratification and that primary production was likely limited by fixed nitrogen availability in the photic zone. Near absence of the C_{30} sterane marine algal biomarker, 24-*n*-propylcholestane (24-npc), in most samples supports and extends the previously observed hiatus of 24-npc in Early Paleozoic (Late Cambrian to Early Silurian) marine environments. Very high abundances of 3β-methylhopanes (average = 9.9%; maximum of 16.8%), extends this biomarker characteristic to Early Ordovician strata for the first time and may reflect enhanced and sustained marine methane cycling during this interval of fluctuating climatic and low sulfate marine conditions. Olenid trilobite fossils are prominent in strata deposited during an interval of marine transgression with biomarker evidence for episodic euxinia/anoxia extending into the photic zone of the water column.

Keywords – Early Ordovician, Middle Ordovician, GOBE, carbon isotopes, nitrogen isotopes, methane cycling

1. Introduction

The Paleozoic Eon was marked by two major episodes of diversification. The first one occurred in the Cambrian and is known as the 'Cambrian Explosion', during which most of the major metazoan groups with mineralised skeletons first appear in the fossil record. The second occurred in the Ordovician and is known as the Great Ordovician Biodiversification Event (GOBE; Sepkoski et al., 1981; Droser & Finnegan, 2003; Webby et al., 2004; Servais & Harper, 2018). During the GOBE, many of the groups that dominated marine ecosystems until the Permian-Triassic mass extinction diversified and rose to ecological dominance. The diversification was accompanied by a variety of major ecological changes including i) increased tiering of benthic

ecosystems (Bottjer & Ausich, 1986), ii) re-establishment of metazoan-dominated reefs (Kröger et al., 2017a), iii) expansion of nektonic and pelagic ecosystems (Servais et al., 2008; Kröger et al., 2009; Servais et al., 2015), and iv) establishment of a latitudinal diversity gradient (Kröger, 2018). Although the timing of diversification varied across clades and from region to region, much of the diversity increase occurred during the Early and Middle Ordovician, especially between the Dapingian (470 Ma) and Darriwilian (467 Ma) stages (Miller & Foote, 1996; Miller, 1997; Droser & Finnegan, 2003; Rasmussen et al., 2016; Trubovitz & Stigall, 2016; Kröger, 2018).

A variety of inter-related extrinsic drivers have been invoked to explain aspects of the GOBE, including i) climatic cooling (Trotter et al., 2008; Rasmussen et al., 2016; Kröger, 2018), ii) increasing oxygenation of the oceans (Saltzman et al., 2015; Edwards et al., 2017) and associated changes in carbonate saturation state (Pruss et al., 2010), and iii) increased volcanic and erosional nutrient flux (Miller & Mao, 1995; Vermeij, 1995; Allmon & Martin, 2014). The Late Cambrian to Early Ordovician rise of acritarch diversity (Servais et al., 2015), followed by diversification of suspension-feeding benthic and planktonic organisms in the Early and Middle Ordovician (Servais et al., 2008), suggests that changes in the amount and/or nature of primary production may have played an important role in the GOBE. However, relatively little is known about the broad structure of marine microbial communities through this period, such as the balance of algal versus bacterial primary producers.

Previous organic geochemical and isotopic investigations of rocks from the Ordovician Period have focused largely on intervals of the Middle Ordovician (Hatch et al., 1987; Foster et al., 1989, 1990; Summons & Jahnke, 1990; Pancost et al., 1998, 1999; Ambrose et al., 2001; Edwards et al., 2013; Spaak et al., 2017), and the Late Ordovician (Rohrssen et al., 2013; Mustafa et al., 2015; Smolarek et al., 2017). Oil shales of the Middle Ordovician (Estonian kukersites;

Mastalerz et al., 2003) and carbonate reservoirs containing oil source rocks from the United States (Guthrie & Pratt, 1995) and northwest China (Tarim Basin; e.g., Cai et al., 2009; Pang et al., 2013; Xiao et al., 2016) are of economic importance. Interest in the Late Ordovician to Early Silurian comes from understanding the mechanisms and climatic drivers that led to the Late Ordovician Hirnantian glaciation (Delabroye & Vecoli, 2010; Finnegan et al., 2011; Luo et al., 2016) and the Late Ordovician Mass Extinction (LOME; LaPorte et al., 2009; Rohrssen et al., 2013; Luo et al., 2016; Zou et al., 2018).

In contrast, the organic geochemical characteristics of Early-Middle Ordovician sedimentary rocks have undergone less scrutiny until now. Previous biomarker studies have focused on facilitating improved oil-source correlations for petroleum fluids expelled from the Cambro-Ordovician Alum Shale in Sweden (Dahl et al., 1989) and from source rocks from central Australia (Summons & Powell, 1991; Jarrett et al., 2016) and the Tarim Basin in China (Li et al., 2000; Cai et al., 2009; Chen et al., 2018 and references therein). Broader goals of this study were then to help bridge a gap in the ancient biomarker record through an important Early-Middle Ordovician interval and to investigate relationships between microbial community structure and nutrient cycling. Here we present a detailed lipid biomarker and stable isotopic investigation of a near-continuous section of well-preserved carbonate-rich sedimentary rocks from the eastern terrane of Ny-Friesland, Spitsbergen, Norway (Figure 1).

2. Geological setting and sampling

The Hinlopenstretet Supergroup contains the Precambrian and Paleozoic successions in the eastern terrane of the Ny-Friesland area in Spitsbergen, Norway (Figure 1). The Paleozoic

Oslobreen Group unconformably overlies Neoproterozoic glacial sediments of the Precambrian Polarisbreen Group (Halverson, 2011). The Cambro-Ordovician section of the Oslobreen Group contains the Cambrian Tokammane Formation and the Early-Middle Ordovician Kirtonryggen and Valhallfonna Formations. These sections have been well studied stratigraphically and paleontologically (e.g., Fortey & Brunton, 1973; Fortey & Cocks, 2003; Brandl, 2009; Stouge et al., 2011; Lehnert et al., 2013; Kröger et al., 2017b and references therein) but high resolution geochemical (either molecular or isotopic) characterisation for this succession is sparse (Brandl, 2009).

Figure 1A shows the study area and sampling site with magnified inset (Figure 1B), which has been previously described in detail by Kröger et al., 2017b and references therein. Samples were collected from three different locations (Figure 1B) during the field expedition in the northern hemisphere summer of 2016. For lipid biomarker and stable isotope analyses, ten samples total were taken from the Kirtonryggen Formation—two from the Spora Member (Spora River), five from the Basissletta Member, and three from the Nordporten Member. 20 sedimentary rocks in total were sampled from the Valhallfonna Formation—18 samples were collected at higher resolution (every 9.2 metres, on average) from the Olenidsletta Member with and additional two samples from the uppermost Profilbekken Member. Lithological description of all samples are provided in Supplementary Table 1 with complementary detailed stratigraphic column shown in Figure 1D.

2.1 Kirtonryggen Formation

The Kirtonryggen Formation (deposited during the Tremadocian-Floian stages, 485-470 Ma) contains the Spora, Basissletta, and Nordporten Members. The Spora Member of the

Kirtonryggen Formation contains mostly planar-bedded limestone and wavy-bedded dolostones containing trilobite, gastropod, and cephalopod fossils (Figure 1D). The Basissletta Member that overlies the Spora Member shows a similar lithology at its base. The middle Basissletta Member displays a change in lithology as it contains horizons of flat pebble conglomerates and intraclastic conglomerates in the middle of the section. In contrast, the uppermost Basissletta Member contains stromatolitic and oolitic facies and planar-bedded limestone. The Basissletta Member is in turn overlain by the Nordporten Member, which is composed of mainly wavy-bedded dolostone with argillaceous/shaly and intraclastic conglomerate layers in between. The middle of the Nordporten Member contains a silty section with trilobite and cephalopod fossils. The upper Nordporten Member continues to be dominantly wavy-bedded dolomite containing trilobite, gastropod, and cephalopod fossils.

2.2 Valhallfonna Formation

The Valhallfonna Formation (deposited during the Floian-Darriwilian stages, 470-458 Ma) contains the Olenidsletta and Profilbekken Members. The base of the Olenidsletta Member contains the cephalopod-rich wavy-bedded dolostone from the Nordporten Member and transitions into densely laminated, mixed dark limestone and black mudstones/bituminous shales throughout the entire sequence with a decrease in the abundance of marine fossils (Figure 1D). The deposition of this interval is interpreted to coincide with a local basin deepening and this succession contains rocks with higher organic carbon content than the underlying Kirtonryggen Formation. The lower and middle Olenidsletta Member contains mixed dark limestone and black mudstones and contains trilobites throughout (mostly in the lower part of the section) and sparingly through the middle. The upper Olenidsletta Member sees the return of wavy-bedded dolostones, hardgrounds, and flint nodules (Kröger et al., 2017b) including abundant inarticulate brachiopods. This fossiliferous

section of the Olenidsletta Member corresponds to the V2a and V2b trilobite biozones with olenid trilobites prominent (Fortey, 1980), the *Oepikodos intermedius* conodont biozone (Lehnert et al., 2013), and the *Didymograptus bifidus* and *Isograptus victoriae lunatus* graptolite biozone (Cooper & Fortey, 1982). The top of the Olenidsletta Member (before the transition into the Profilbekken Member) returns to the composition of the lower/middle Olenidsletta Member. The Profilbekken Member is similar in depositional environment and lithological composition to the Nordporten Member from the Kirtonryggen Formation (Kröger et al., 2017b), containing planar-bedded limestone with trilobites, cephalopods, and inarticulate brachiopods.

3. Methods

3.1 Sample preparation

Outcrop samples were collected, wrapped in pre-combusted (550°C, 9 hours) aluminium foil and stored in cloth bags. Outer portions of each sample were removed with a water-cooled diamond saw and inner portions were sonicated three times for 15 mins each in rinses of deionised water (DI), dichloromethane (DCM), methanol, (MeOH), *n*-hexane, and DCM. Each solvent rinse was discarded prior to rinsing with the next solvent. Cleaned rock samples were crushed using an organic solvent-cleaned zirconia ceramic puck mill in a 8515 SPEX Shatterbox with a procedural blank of pre-combusted (850°C, 9 hours) sand. Combusted quartz sand blanks were run parallel with the extracted rock powders as full analytical procedural blanks as an important control to monitor background contamination.

3.2 Bulk organic carbon and nitrogen isotopes

For isotopic analysis, samples were decarbonated with 1 M HCl to remove any carbonate material prior to isotopic measurement of the organic material. Samples and standards were

weighed out on a Mettler Toledo microbalance (ranging from 5 mg to 40 mg depending upon organic content) and loaded into the EA autosampler. The remaining organic residue was measured for bulk carbon ($\delta^{13}C$) and nitrogen ($\delta^{15}N$) isotope signatures using an Elementar Isotope Select cube elemental analyser (EA) coupled to a VisION isotope ratio mass spectrometer (IRMS). All samples for carbon and nitrogen were run in triplicate, with stable isotope results reported as $\delta^{13}C$ relative to VPDB in permil (‰) and calibrated using certified international standards (USGS24 & NBS22). The measured standard deviation for all carbon isotope measurements is ±0.1‰. Stable isotope results are reported as $\delta^{15}N$ relative to air in permil (‰) and calibrated using certified international standards (USGS25, IAEA-N-1 & IAEA-N-2). The measured standard deviation for all nitrogen isotope measurements is ±0.2‰.

3.3 LECO Total Organic Carbon (TOC) and Rock-Eval Pyrolysis analyses

To determine TOC contents, the decarbonated samples were analysed at GeoMark Research using a LECO C230 instrument. The LECO C230 instrument was calibrated with standards that have known carbon contents. Standards were combusted by heating to 1200°C in the presence of oxygen; both carbon monoxide (CO) and carbon dioxide (CO_2) were generated and the CO was converted to CO_2 by a catalyst. The CO_2 product mass was measured by an IR cell. Combustion of samples with unknown organic carbon content was then completed and the response of these samples per mass unit was compared to that of the calibration standard. Standards were analysed every 10 samples to check variation and calibration of the analysis. Acceptable standard deviation for TOC is 3% variation from established value.

Approximately 100 mg of washed, ground (60 mesh) whole rock sample were analysed in a Rock-Eval II instrument. Measurements include S1: free bitumen content (mg HC/g rock); S2:

remaining generation potential (mg HC/g rock); Tmax: temperature at maximum evolution of S2 hydrocarbons (°C); and S3: organic carbon dioxide yield (mg CO_2/g rock), and were generated by heating according to the following parameters S1: 300°C for 3 minutes; S2: 300°C to 550°C at 25°C/min, held at 550°C for 1 minute; S3: trapped between 300 to 390°C. Instrument calibration was achieved using a rock standard with values determined from a calibration curve to pure hydrocarbons of varying concentrations.

3.4 Sample extraction

10-30 g of rock powder per sample was extracted in organic solvent-cleaned Teflon vessels on a CEM MARS5 microwave accelerated reaction system in 30 ml of 9:1 (v/v) DCM/MeOH. Samples were heated to 100°C for 15 mins with constant stirring. Procedural blanks were performed with combusted silica. Rock bitumens were filtered and desulfurised with solvent-cleaned and HCl-activated copper granules (Alfa Aesar). Saturated, aromatic, and polar hydrocarbons were obtained through fractionation on dry-packed silica gel (Fisher, 60 grit) microcolumns. The silica gel was combusted in a muffle furnace at 450°C for at least 9 hours to remove any organic contaminant residue prior to adsorption of whole rock extracts and use in column chromatography. The saturated hydrocarbon fraction eluted with 1 dead volume (DV) of *n*-hexane, aromatic hydrocarbons with 3 DVs of 1:1 (v/v) *n*-hexane:DCM, and the polar hydrocarbons with 2 DVs of 3:1 (v/v) DCM:MeOH.

3.5 Gas Chromatography-Mass Spectrometry (GC-MS)

The saturated and aromatic hydrocarbon fractions were run in full scan and selected ion monitoring (SIM) mode on an Agilent 7890A GC system coupled to an Agilent 5975C inert MSD mass spectrometer. The GC was equipped with a DB1-MS capillary column (60 m × 0.32 mm, 0.25 μm film thickness) and He was used as the carrier gas. The GC temperature program used was 60°C (held for 2 min), heated to 150°C at 20°C/min, then to 325°C at 2°C/min, and held at 325°C for 20 mins. Pristane/phytane (Pr/Ph) ratios were measured from relative peak areas using total ion current (TIC) chromatograms acquired from full scan analysis. Chlorobi-derived carotenoid biomarkers, including aryl isoprenoids, isorenieratane, and paleorenieratane were identified based on 133 and 134 Dalton (Da) mass chromatograms, with 3,4,5- and 2,3,6-trimethyl-substituted aryl isoprenoid abundances measured from peak areas in 133 Da ion chromatograms, with isorenieratane and paleorenieratane verified from mass spectra and retention times.

3.6 Gas Chromatography-Metastable Reaction Monitoring (GC-MRM)

Saturated hydrocarbons were analysed in metastable reaction monitoring (MRM) mode on a Waters AutoSpec Premier equipped with an Agilent 7890 gas chromatograph (GC). The GC was equipped with a DB1-MS capillary column (60 m × 0.25 mm, 0.25 μm film thickness) and He was used as the carrier gas. Samples were run in full scan mode and injected into the GC in splitless mode at 60°C for 2 min, heated at 10°C/min to 150°C, then 3°C/min to 320°C for 22 mins. Analyses were performed in electron impact mode with 70 eV ionisation energy and 8 kV accelerating voltage. MRM transitions for C_{27}-C_{35} hopanes, C_{31}-C_{36} methylhopanes, C_{21}-C_{22} and C_{26}-C_{30} steranes, C_{30} methylsteranes and C_{19}-C_{26} tricyclics were monitored in the method used. Procedural blanks with pre-combusted sand yielded less than 0.1 ng of individual hopane and sterane isomers per gram of combusted sand. Polycyclic biomarker alkanes (tricyclic terpanes, hopanes, steranes, etc.) were quantified by addition of 50 ng of deuterated C_{29} sterane standard

[d4-ααα-24-ethylcholestane (20R), Chiron Laboratories] to saturated hydrocarbon fractions and by comparison of relative peak areas. MRM-GC-MS was used to determine accurate biomarker abundance ratios for all the polycyclic biomarkers plotted in Figures 2, 4, and 5. Analytical error for individual hopane and sterane concentrations are estimated at ± 30%. Average uncertainties in hopane and sterane biomarker ratios are ± 8% as calculated from multiple analyses of saturated hydrocarbon fractions from oil standards.

4. Results

Chemostratigraphic records were obtained by integrating geochemical data from sedimentary strata from three different outcrop sections spanning two formations of the Oslobreen Group—the upper Valhallfonna Formation (Olenidsletta Member as denoted by PO and Profilbekken Member as denoted by PR) and the underlying Kirtonryggen Formation (all samples from Spora, Basissletta, and Nordporten Members denoted by PS). The raw geochemical data used to construct the stratigraphic plots shown in Figures 2-5 are available in Supplementary Tables (3-6). Younger biomarkers (oleanane, oleanane triterpanes, bicadinane, and taraxastane), plastic-derived hydrocarbons (e.g., branched alkanes with quaternary carbon centres, BAQCs), and other obvious contaminants are absent in all samples. The distinctive Ordovician patterns evident in the biomarker assemblages and the robust stratigraphic trends in biomarker ratios are generally consistent with the age, thermal maturity and lithology of the host rocks, which is an important self-consistency check that supports biomarker syngenicity for our sample set.

4.1 Thermal maturity proxies

Selected saturated and aromatic hydrocarbon maturity ratios alongside Tmax from Rock Eval pyrolysis (values listed in Supplementary Table 3), placing these samples in the mid-oil window range of thermal maturity, but prior to peak generation, and with a generally consistent thermal maturity profile observed throughout the section (Figure 2). A Tmax range from 441 to 446°C for samples from the Olenidsletta Formation (PO; Figure 2A), methylphenanthrene index (MPI) in the range of 0.4 to 1.0 (average = 0.73, Figure 2B), average C_{29} ααα sterane (20S/20S+20R) of 0.51 ± 0.04 (Figure 2D), and average C_{31} αβ hopane (22S/22S+22R) of 0.58 ± 0.01 are all consistent with this assessment. Ts/Ts+Tm ratios for C_{27} hopanes (Figure 2C) are fairly low and constant throughout the Profilbekken and Olenidsletta Members (average of 0.36 ± 0.05) but are consistently higher (average of 0.54 ± 0.12) in the underlying Kirtonryggen Formation, which is more thermally mature (Supplementary Table 3).

4.2 Organic and inorganic carbon content and bulk stable carbon and nitrogen isotopes

All sedimentary rocks analysed in this study contain high carbonate content (wt%), (Figure 3A) with an overall range of 53 to 99 wt% of the bulk mass. At the top of the Nordporten Member of the Kirtonryggen Formation (the boundary between the Nordporten and the deeper water strata of the Olenidsletta Member), there is a decrease in carbonate content as the lithology becomes mixed with siliciclastic minerals (mudstone and siltstone). Carbonate content then increases again stratigraphically higher into Profilbekken Member shallow water carbonates (Kröger et al., 2017b). TOC content is generally low for most of the Kirtonryggen Formation (most samples with <0.1 wt%; Figure 3B) but increases to 2.5 wt% at the top of the unit in samples from the Olenidsletta Member of the Valhallfonna Formation (TOC ranging from 0.2 to 3.8 wt%), with two noticeable spike increases around the base and at the top of this succession, which throughout is

generally associated with a deeper shelf depositional setting than the underlying and overlying strata.

Bulk organic carbon isotopes through the Kirtonryggen and Valhallfonna Formations are stable, showing little variation throughout (average -30.4‰ ± 0.8‰; Figure 3C) and typical of bulk organic carbon values for Paleozoic sedimentary rocks (Hayes et al., 1999). There is a slight decreasing trend toward lighter $\delta^{13}C_{org}$ values from the base of the Basissletta Member up to the Basissletta/Nordporten boundary representing a small variation of ca. 2‰ in magnitude. $\delta^{13}C_{org}$ values return to a heavier baseline of -29‰ at the Nordporten/Olenidsletta boundary with another small, (ca. 2‰) negative excursion through to the upper portion of the Olenidsletta Member, followed by a low magnitude recovery to ca. -30‰. Bulk nitrogen isotopes ($\delta^{15}N_{total}$) are most enriched in $\delta^{15}N$ in the Basissletta Member (average of +1.5‰) and experience a ca. 2.4‰ negative excursion (down to -1‰) at the Nordporten/Olenidsletta boundary coinciding with higher TOC content (Figure 3D). $\delta^{15}N_{org}$ values then increase again to ca. +1‰ moving from the Nordporten/Olenidsletta boundary into the overlying Profilbekken Member. Overall, the average $\delta^{15}N_{total}$ signature for all data points is near zero in value (+0.4‰), close to the typical ancient sedimentary bulk nitrogen isotope values associated with a bacterial nitrogen fixation (ca. 0 to -1‰) signature (Delwich & Steyn, 1970).

4.3 Saturated hydrocarbon biomarkers

Saturated hydrocarbon profiles of these Oslobreen Group carbonates generally contain abundant *n*-alkanes and alkylcyclohexanes with only a slight odd-over-even (OEP) carbon number preference, but no strong *G. prisca* (*Gloeocapsomorpha prisca*; nC$_{15}$, nC$_{17}$, and nC$_{19}$ alkane carbon number preference) molecular signature is discernible. Pristane and phytane are the dominant

isoprenoids and methylalkanes are generally low in abundance relative to the dominant *n*-alkanes. The most abundant polycyclic biomarker alkanes include tri- and tetracyclic terpanes, steranes, hopanes, and methylhopanes. Saturated hydrocarbons show variable contents of unresolved complex mixtures (UCMs) from sample to sample (e.g., Supplementary Figure 1). Carbonates from the Profilbekken Member and the Kirtonryggen Formation have small or no UCMs, whereas samples from the Olenidsletta Member have small and moderate to larger UCMs. Although reasons for this are not entirely clear, enhanced UCMs in Ordovician rocks are generally associated with more reducing environmental marine conditions which is reminiscent of the prominent UCM features of saturated hydrocarbons profiles from immature Mesoproterozoic marine rocks rich in bacterial source inputs and deposited in low oxygen marine conditions (e.g., Pawlowska et al., 2013).

Hopane/sterane ratios show a declining trend from very high values (ca. 13) at the base of the Basissletta Member (Figure 4B) to values slightly higher (ca. 2.2) than the upper boundary value of the Phanerozoic marine average at the Nordporten/Olenidsletta boundary. Through the Olenidsletta Member, hopane/sterane ratios increase to average values of 6.4 in the Profilbekken Member. Total sterane (sum of C_{27}-C_{29} regular steranes and diasteranes) concentrations are lower (0.8 to 13 ppm TOC) in the Kirtonryggen Formation compared with the upper Valhallfonna Formation (4 to 50 ppm TOC) (Supplementary Table 2). C_{29} steranes are the dominant steranes which is typical for Paleozoic sedimentary rocks and oils (e.g., Schwark & Empt, 2006; Haddad et al., 2016), followed by C_{27} and C_{28} (Figure 4E). C_{28}/C_{29} sterane ratios have moderate values throughout the entire section, showing little variation with stratigraphic position (Figure 5B; average 0.5 ± 0.1). C_{30} steranes are either very low in abundance or below detection limits. C_{30} steranes are below detection limits in all Kirtonryggen Formation samples and appear in small

quantities (both 24-*n*-propylcholestane and 24-isopropylcholestane; 24-npc and 24-ipc, respectively) in select Olenidsletta Member samples (Supplementary Table 5). Total C_{27}-C_{35} hopane concentrations in the Kirtonryggen Formation (7 to 102 ppm TOC) are similar to the same range as the upper Valhallfonna Formation (7 to 144 ppm TOC), but overall slightly lower than the middle to lower Valhallfonna Formation (Supplementary Table 2). C_{29}/C_{30} hopane ratios are quite high (average = 0.95) as is typical for sedimentary rocks with high carbonate mineral content (Peters et al., 2005; Figure 5C).

Methylhopanes, both 2α- and 3β- (sum of C_{31}-C_{36}), are present and abundant in all samples from the Oslobreen Group (Figure 4C, 4D and Figure 6). Both exhibit similar concentrations throughout the section, with slightly higher values of 3β-methylhopanes in the Olenidsletta and Profilbekken Members (Figure 4C, 4D and Supplementary Table 2). Absolute abundances of 2α- and 3β-methylhopanes in the Kirtonryggen and Valhallfonna Formations range from 0.1 to 3 ppm TOC. Methylhopane indices (MeHI) were calculated for the C_{31} homologue of 2α-methylhopane and 3β-methylhopane (expressed as a percentage value from C_{31} αβ MeH/C_{31} αβ MeH +C_{30} αβ hopane). The 2α-methylhopane trend shows an initial decrease at the base of the Spora Member with recovery to higher values in the Basissletta Member. Upsection through the Nordporten Member, 2α-methylhopane indices (2MeHI) drop to ca. 5 and recover to ca. 10 at the Nordporten/Olenidsletta boundary (Figure 4C). Through the more organic-rich Olenidsletta Member, the 2MeHI remains constant with most values around 5% (average 5.6% ± 1.6%). 3β-methylhopane indices (3MeHI) show a range of values (3 to 17%) but are generally high in magnitude (Figure 6) and consistently above typical Phanerozoic marine average values (1 to 3%). At the base of the Olenidsletta Member, there is an increase in 3MeHI (from 3% to 13%) moving stratigraphically upwards into strata with higher TOC contents. Additionally, acyclic biphytane

(C_{40}) from archaea was found in most of the Olenidsletta Member samples (Supplementary Table 7) and in trace amounts in two samples from the lower Basissletta Member and lower Nordporten Member of the Kirtonryggen Formation. The relative abundance of acyclic biphytane to *n*-alkanes (nC_{35}) in Olenidsletta Member samples is highest in the upper Valhallfonna Formation. Other C_{40} cyclic (mono-, bi-, and tri- cyclic biphytanes) were found in six Olenidsletta Member samples and in trace quantities in five samples throughout the section (Supplementary Figures 2 and 3). These are below detection limits in samples from the Kirtonryggen Formation.

Figure 4G shows the gammacerane index (calculated as gammacerane/C_{30} αβ hopane) exhibiting mostly low values through the Olenidsletta, Nordporten, and the upper and middle Basissletta Members, which is consistent with a normal marine salinity environment (Peters et al., 2005) and no strong water column stratification related to salinity during the deposition of rocks with appreciable TOC content. The exception is for the organic-lean Basissletta/Spora Member carbonates deposited in more saline and restricted environments, exhibiting values up to 0.7 in the Spora Member. Other selected biomarkers indicative of paleoenvironmental and paleoredox depositional conditions, such as Pr/Ph (pristane/phytane), homohopane index (HHI%; as (C_{35}/C_{31}-C_{35})*100)), C_{28} bisnorhopane (28BNH/C_{30} αβ hopane), and dibenzothiophene/phenanthrene (DBT/P) are shown in Figures 5D-5G. Pr/Ph values increase from ca. 0.5 at the base of the Kirtonryggen Formation to 1.2 in the Nordporten Member and decrease to low values (ca. 0.5) in the middle of the Olenidsletta Member. Values recover to ca. 1.0 in to the Profilbekken Member (Figure 5D). The homohopane index (HHI; Figure 5E), C_{28} bisnorhopane (Figure 5F), and DBT/P (Figure 5G) all show antithetical relationships to Pr/Ph values. These particular proxies increase markedly in the middle of the Olenidsletta Formation, which is the more organic-rich strata and

likely associated with deposition during marine transgression sustaining a redox-stratified water column, whilst remaining low and invariable in the rest of the strata.

4.4 Aromatic hydrocarbon biomarkers

All aromatic hydrocarbon fractions contain a variety of 1 to 7 ring polyaromatic hydrocarbons (PAHs) including phenanthrene, alkylphenanthrenes, dibenzothiophenes, benzofluoranthenes, benzopyrenes, and coronenes, and contain large UCMs in full scan and selected ion monitoring (SIM) mode. Additionally, mono- and triaromatic steroids are also present in all samples. Almost all samples from the Valhallfonna Formation with appreciable TOC contents (>0.3%) contain paleorenieratane, isorenieratane, and 2,3,6- and 3,4,5-trimethylarylisoprenoids (in samples where paleorenieratane is higher than isorenieratane). Figure 7 shows partial ion chromatograms (*m*/*z* 134 and 546) of isorenieratane (I; Figure 7A) and paleorenieratane (P) and trimethylaryl isoprenoid fragments (Figure 7B) in a sample from the Profilbekken Member. Two samples from the Profilbekken Member (PR-6 and PR-30.4) and most samples from the Olenidsletta Member contain higher relative amounts of isorenieratane than paleorenieratane (I > P; Figure 4F). The most striking trend observed is for strata near the base of the Olenidsletta Member which contain significantly greater amounts of paleorenieratane compared to isorenieratane (P/I > 2). This corresponds to a switch to increasing TOC content of the host rocks and a likely deeper water and open marine depositional environmental setting due to local sea level rise. Aromatic carotenoids and arylisoprenoid fragmentation products were below detectable limits in all samples from the Kirtonryggen Formation. Other carotenoids, such as β-carotane, γ-carotane, lycopane, okenane, and chlorobactane, were below detectable limits in all samples.

5. Discussion

The biomarker assemblages and their implication for biological source inputs and paleoenvironmental settings

The organic geochemical and stable isotopic characteristics of Early-Middle Ordovician carbonates from Spitsbergen exhibit some broad characteristics similar to those reported previously from Middle-Late Ordovician marine settings (e.g., Rohrssen et al., 2013; Spaak et al., 2017), albeit with some deviations likely due to local overprint effects, such as organic matter source inputs and local paleoenvironments. Ordovician marine sedimentary rocks and oils often contain low acyclic isoprenoids abundances, elevated hopane/sterane ratios, high 3β-methylhopanes, as found also for our sample set (e.g., Fowler & Douglas, 1984; Jacobsen et al., 1988; Summons & Jahnke, 1990; Rohrssen et al., 2013; Spaak et al., 2017).

In terms of major alkane constituents, the rock extracts from the Oslobreen Group are dominated by a marine *n*-alkane signature (extending from nC$_{15}$ up to nC$_{40}$) that begin to tail off in abundance with increasing carbon number above nC$_{22}$ (Supplementary Figure 1). The *n*-alkanes and alkylcyclohexane abundance profiles in all our rock extracts do not have the pronounced *G. prisca* signature (Fowler & Douglas, 1984), namely a readily discernible carbon number preference for low molecular weight odd carbon numbered *n*-alkanes and alkylcyclohexanes. Some samples show carbon number preference for low molecular weight odd carbon numbered *n*-alkanes and alkylcyclohexanes (nC$_{15}$, nC$_{17}$, and nC$_{19}$) enhanced in *m*/*z* 83 and *m*/*z* 85 ion chromatograms, respectively. The lack of a pronounced *G. prisca* signature in *n*-alkanes has also been observed in other Ordovician source rocks (e.g., Fowler, 1992; Sun et al., 2013; Rohrssen et

al., 2013). In our rock set, the major organic matter source input appears to be dominated by amorphous marine Type II kerogen derived mainly from mixed autochthonous bacterial and algal sources.

The C_{29} steranes commonly comprise the most abundant sterane signal throughout the section with an average value of 44%, although the C_{27} steranes become slightly higher in a restricted interval for organic-lean strata within the Nordporten Member (Figure 4E). However, the magnitude of the C_{29} sterane dominance is overall lower in our sample set than previously reported for other Early Paleozoic paleotropical settings of Late Ordovician (Rohrssen et al., 2013) and Late Devonian (Haddad et al., 2016; Martinez et al., 2018) age. The proportion of C_{28}/C_{29} steranes, which average ca. 0.5 in this study (expected for Paleozoic rocks), is also higher than the average values of ca. 0.3 for paleotropical marine settings in the Late Ordovician (Rohrssen et al., 2013) and the Late Devonian (Haddad et al., 2016). The enhanced proportions of C_{28} and C_{27} sterane biomarkers suggest that prasinophyte algae and other algal groups existed as significant contributors to preserved organic matter along with the C_{29} sterol-producing green algal clades (Schwark & Empt, 2006; Kodner et al., 2008; Haddad et al., 2016).

Hopanes methylated at the C-3 position are typically low in abundance relative to the regular hopane series in most Phanerozoic marine sedimentary rocks (usually within a tight range of 1-3% of C_{30} αβ hopane; Peters et al., 2005; Cao et al., 2009; Rohrssen et al., 2013), but have been found to be moderately to highly elevated during certain periods in Earth history associated with low marine sulfate conditions; e.g., in the Paleoproterozoic (Brocks et al., 2005), the Mesoproterozoic (Blumenberg et al., 2012), the Middle Ordovician (Spaak et al., 2017), the Late Ordovician-Silurian (Summons & Jahnke, 1990; Rohrssen et al., 2013), and the Late Permian (Cao et al., 2009). Biological precursors of 3β-methylhopanoids include diverse groups of

proteobacteria (Welander & Summons, 2012), although microaerophilic proteobacteria (typically Type I methanotrophic bacteria) are usually invoked as a major source (Farrimond et al., 2004). This is supported by ^{13}C-depletion in 3β-methylhopanes from compound-specific carbon isotope measurements of ancient rocks containing abundant 3β-methylhopanes (Collister et al., 1992; Ruble et al., 1994). A likely source of the relatively abundant 3β-methylhopanes in Oslobreen Group marine carbonates is from methanotrophic bacteria as for Late Ordovician strata (Rohrssen et al., 2013).

In addition to abundant 3-methylhopanes, we detected acyclic biphytane in most of the samples from the Olenidsletta Member and in trace quantities in one Basissletta and one Nordporten Member sample (Supplementary Table 6). Additionally, 11 samples from the Olenidsletta Member contained trace but detectable amounts of mono-, bi-, and tricyclic biphytanes (the latter constituting a cluster of peaks, suggesting some cyclic groups were the result of diagenetic and catagenetic alteration with prominent *m*/*z* 263 fragment ion; Supplementary Figure 2 and 3; DeLong et al., 1998). Although intact acyclic biphytane is rarely found preserved in ancient sedimentary rocks and oils (Saito et al., 2017; Schinteie & Brocks, 2017), a recent study has found acyclic biphytane and associated degradation products in sedimentary rocks deposited in a Neoproterozoic hypersaline ecosystem (Schinteie & Brocks, 2017). At 820 Ma, this constitutes the oldest occurrence of acyclic biphytane in the geological record, likely derived from the membranes of halotolerant archaea. Acyclic biphytane preserved in the Oslobreen carbonates of the Early-Middle Ordovician in this study thus far presents the oldest reported occurrence of acyclic biphytane preserved under conventional marine salinity conditions (as supported by generally low gammacerane index values), and is sourced from archaea, with the previous oldest occurrences in the Jurassic/Cretaceous (Kuypers et al., 2001; Carrillo-Hernandez et al., 2003). The

high UCMs in the high molecular weight region of our samples, combined with low absolute abundances of acyclic biphytane, precludes the possibility of obtaining accurate and reproducible compound-specific carbon isotope ratio values for biphytane. Although given the overall biomarker characteristics, the co-occurrence of acyclic biphytane and trace amounts of cyclic biphytanes along with high 3MeHI values suggest that an enhanced microbially-driven methane cycle likely occurred in this low marine sulfate environment. In this scenario, biphytane could be derived from methanotrophic and/or methanogenic archaea (Kuypers et al., 2001) with the abundant 3β-methylhopanes largely sourced from microaerophilic methanotrophic bacteria. Previously, elevated 3β-methylhopanes have been reported from samples from the Late Ordovician of Laurentia and Baltica (Rohrssen et al., 2013) and more recently from the Middle Ordovician of Gondwana (Spaak et al., 2017). Overall, methanotrophic microorganisms appear to be largely contributing to the bitumen composition, pointing to enhanced and sustained methane cycling occurring during the Ordovician as suggested previously (Rohrssen et al., 2013). This active methane cycle has potential implications for climate and climate feedbacks in the Middle and Late Ordovician.

Lipid biomarker ratios provide information about the redox state of the environment in which organic matter was deposited. Figure 5D-5G displays stratigraphic trends for Pr/Ph, homohopane index (HHI), C_{28} bisnorhopanes, and dibenzothiophene/phenanthrene (DBT/P) and shows that the Olenidsletta Member—thought to be deposited during a local deepening of the basin (Kröger et al., 2017b)—was deposited under redox-stratified water column conditions, which is supported by the higher TOC contents observed in this section. A cross-plot of the arylisoprenoid ratio (AIR; C_{13}-C_{17}/C_{18}-C_{22} arylisoprenoids) and Pr/Ph indicate that these samples were seemingly deposited under persistently anoxic conditions in the photic zone (as defined in Schwark &

Frimmel, 2004; Supplementary Figure 4), although the upper surface mixed layer must have remained oxygenated within a redox stratified water column. Carotenoids and their arylisoprenoidal degradation products have been reported previously in Early-Middle Ordovician samples (Cai et al., 2009; French et al., 2015) and are expected for locally productive continental margin settings sustaining photic zone euxinia in the lower portion of the photic zone (down to ca. 100 m depth). The presence of trimethylarylisoprenoids (both 2,3,6- and 3,4,5- isomers) along with isorenieratane and paleorenieratane in all Olenidsletta Member samples indicate that, in addition to being anoxic, the water column could have been episodically euxinic in the photic zone.

The major driver of variation in the formations studied are attributed to changes in microbial communities, however, differences in lithologies and paleoredox are also contributing. The depositional environment of the youngest Profilbekken Member is most similar to the upper Nordporten Member—representing open shelf, shallower water carbonates. The lower Kirtonryggen Formation (lower Basissletta Member) represents a facies deposited under more restricted environmental conditions. In this lower strata, we observe high gammacerane index values up to 0.7 at the base of the section which could be pointing to a more saline, stratified environment. Additionally, microbialite and oolite structures are common only in the lower Basissletta Member (Kröger et al., 2017b) and an organic source contribution from benthic microbial mats is anticipated and consistent with the low TOC contents and biomarker assemblages reported for this strata. The Olenidsletta Member is perhaps the most distinctive of all three, being deposited under deeper water conditions during a marine transgression, with enhanced organic matter preservation (as indicated by higher TOC). Lipid biomarkers and nitrogen isotopes indicate that this bacterial-dominated environment was characterised by anoxic and intermittently photic zone euxinic conditions.

496 $\delta^{13}C_{org}$ values—average -30.4‰—from the Oslobreen Group are similar to reports from
497 other Early-Middle Ordovician localities (e.g., Buggisch et al., 2003; Azmy & Lavoie, 2009;
498 Zhang et al., 2010; Edwards & Saltzman, 2016) and close to the average $\delta^{13}C_{org}$ of -29.4‰ for
499 global bulk marine sedimentary organic matter for this time period (Hayes et al., 1999 and
500 references therein). Some sections from South China (Zhang et al., 2010), Ireland (Jahren et al.,
501 2013), and France (Alvaro et al., 2008) report average carbon isotopic values that are, on average,
502 4-6‰ heavier than reported here. However, Jahren et al. (2013) reported ^{13}C-enriched bulk organic
503 matter values in the Ordovician of Ireland (Illaunglass Formation, Tremadocian-Floian stages),
504 these values are 13‰ heavier than the ones measured in the sample set investigated here. It has
505 been proposed from palynological and isotopic evidence that colonisation of primitive land plants
506 prior to the Devonian rise of vascular land plants (Middle Ordovician; Strother et al., 1996;
507 Tomescu et al., 2009; Rubinstein et al., 2010; Spaak et al., 2017) may be a possible explanation
508 for these anomalously ^{13}C-enriched bulk isotopic values (Tomescu et al., 2009; Jahren et al., 2013).
509 Such signature contributions are not evident in bulk $\delta^{13}C_{org}$ values from the Early-Middle
510 Ordovician strata of Spitsbergen.

511 *High bacterial contributions to preserved organic matter*

512 The ratio of the sum of all the major hopane versus sterane constituents (H/St) gives a broad
513 but informative guide to the overall balance of bacterial versus eukaryotic source contributions to
514 preserved sedimentary organic matter and can be accurately measured from MRM-GC-MS. The
515 Phanerozoic marine average for organic-rich sedimentary rocks and oils for (H/St) ratio typically
516 falls in the range of 0.5 to 2.0 (Peters et al., 2005; Rohrssen et al., 2013). The H/St for all of our
517 Oslobreen Group samples are generally above the upper limit of the marine Phanerozoic average
518 (upper value of the Phanerozoic average is 2.0, for our samples the average value is 6.4). Values

519 >2 are found even in the deeper water strata with appreciable TOC content of the lower
520 Olenidsletta Member (Figure 4B), indicating a high proportion of bacterial source input
521 contributions to the preserved organic matter during sediment deposition.

522 A series of 2α-methylhopanes are present and abundant in all samples, with most 2MeHI
523 values exceeding 5% (average = 6.6%; Figure 4C). Biological precursors of 2-methylhopanes have
524 previously been linked to oxygenic photosynthesising cyanobacteria (Summons & Jahnke, 1990;
525 Summons et al., 1999) but have subsequently also been found in anoxygenic photoautotrophs and
526 other bacteria (Rashby et al., 2007; Doughty et al., 2009; Welander et al., 2010). While 2α-
527 methylhopanes cannot be used to identify specific biological source organisms (Ricci et al., 2014)
528 they can, however, provide some broad insights into depositional environmental conditions.
529 Intriguing correlations between elevated 2α-methylhopanes and distinctive chemostratigraphic
530 indicators have been noted previously in the geological record. High 2α-methylhopane abundances
531 in the Phanerozoic rock record have previously been associated with the duration or the aftermath
532 of oceanic anoxic events (OAEs) and often, but not always (French et al., 2014), accompanied by
533 shifts in bulk nitrogen isotopes suggesting nitrate limitation (e.g., Kuypers et al., 2004; Cao et al.,
534 2009; Sepúlveda et al., 2009; Luo et al., 2011). This shift in nitrogen isotopic compositions to ^{15}N-
535 depleted (zero to negative) values (Figure 3D) is likely due to the activity of diazotrophic
536 cyanobacteria fixing nitrogen as plankton and/or proliferation of microbial mats. Elevated 2α-
537 methylhopanes combined with low (ranging from -2 to +4‰ but averaging -1 to +1‰ for normal
538 marine salinity facies) $\delta^{15}N_{total}$ values are in general agreement with a stratified and nutrient
539 (nitrate)-limited aquatic environment favouring diazotrophic bacteria. Nitrogen isotope values
540 reported here are similar to those reported in another Early Ordovician section (Azmy et al., 2015)
541 and fixed nitrogen limitation has been commonly associated with Late Ordovician shelf and

basinal settings (e.g., LaPorte et al., 2009; Kiipli & Kiipli, 2013; Luo et al., 2016). The more organic-rich strata of the lower Olenidsletta Member yield $\delta^{15}N_{total}$ signatures which are slightly ^{15}N-depleted by about 1‰ (mostly within the 0 to -1‰ range in Figure 3D) relative to organic-lean rocks. This may signify increased transport of recycled ^{15}N-depleted ammonium back into the water column from sedimentary organic matter during redox stratification for uptake by green algae and other microbial producers, given the higher TOC contents. Overall though, the near zero signatures for $\delta^{15}N_{total}$ are strongly indicative of bioavailable fixed nitrogen being the local limiting nutrient for primary productivity for Oslobreen Group rocks. This is also consistent with the elevated H/St and 2MeHI values that indicate a high contribution of bacterial source organisms.

Implications of extremely low/absent C_{30} regular steranes

An Early Paleozoic hiatus in the occurrence of the C_{30} sterane compound, 24-*n*-propylcholestane (24-npc), in ancient marine environments was proposed previously (Rohrssen et al., 2015). This particular sterane biomarker is often applied to distinguish marine depositional environments, as opposed to lacustrine or highly restricted marine basins. 24-npc is a steroid marker biosynthesised by pelagophyte microalgae for most Phanerozoic rocks and oils of Devonian age and younger (Gold et al., 2016). Possible sources of 24-npc sterane in older Phanerozoic and Neoproterozoic rocks are demosponges (Love et al., 2009) and/or foraminifera (Grabenstatter et al., 2013). Rohrssen et al. (2015) found that 24-npc was low or absent in samples from Middle-Late Cambrian age as well as during an extended interval spanning the Late Ordovician-Early Silurian transition.

We found that 24-npc is below detection limits (estimated as 0.34% of total C_{27}-C_{30} steranes, to take account of prominent UCMs) in samples from the Kirtonryggen Formation and

first appears in trace concentrations beginning near the base of the Olenidsletta Member. Abundance of this compound continues to be present either in trace amounts or below detection limits throughout the Olenidsletta Member but increases slightly at the very top (reaching only up to 0.8% of total C_{27}-C_{30} steranes, continuing into the Profilbekken Member. The first hiatus of C_{30} steranes, reported by Rohrssen et al. (2015), is extended by our results where 24-npc was below detection limits in the Kirtonryggen Formation and part of the Olenidsletta Member. This hiatus is now extended from the Middle Cambrian into the Early Ordovician. 24-npc has been widely reported in Neoproterozoic rocks and oils from different locations (e.g., Love et al., 2008; Love et al., 2009; Grosjean et al., 2009; Kelly et al., 2011; Lee et al., 2013), particularly in eutrophic settings but can also be absent in Neoproterozoic rocks despite the recognition of the characteristic C_{29} sterane dominance (Pehr et al., 2018). It is likely that the source of 24-npc in the Neoproterozoic and Early Paleozoic is derived from demosponges, which also biosynthesise 24-isopropylcholestane (24-ipc), and/or from foraminifera (Grabenstatter et al., 2013) given that marine pelagophyte and their algal ancestors did not likely produce C_{30} sterols until around the Devonian Period as gauged from molecular clock estimates (Gold et al., 2016). Therefore, our samples that contain detectable amounts of 24-npc steranes from the Olenidsletta Member are probably not algal derived, particularly as the 24-ipc biomarker is found in similar abundance to 24-npc (Love et al., 2009; Love & Summons, 2015; Gold et al., 2016).

Potential implications for marine invertebrate taxa during the GOBE

Overall the lipid biomarker assemblages and stable isotopic characteristics for this paleotropical marine shelfal setting, suggest a bacterially-dominated community structure that was influenced and moderated by sea level and ocean connectivity fluctuations, water column redox-stratification during marine transgression, as well as overall nutrient cycle constraints. Fixed

587 nitrogen limitation would have been a commonly important factor influencing the ecology of
588 paleotropical shelf environments during the Early Ordovician, since availability of organic matter
589 for heterotrophic uptake was strongly nutrient-limited.

590 Trilobite faunas during periods of redox stratification (i.e., in the lower and upper
591 Olenidsletta Member, when TOC is high and $\delta^{15}N_{total}$ is low) were exclusively comprised of
592 species belonging to the family Olenidae, a group characteristic of deep-water, low-oxygen
593 conditions in Ordovician sedimentary basins (Farrell et al., 2011), and of putatively pelagic taxa,
594 such as agnostid arthropods and the trilobites *Carolinites* and *Opipeuter* (Fortey, 1974; Fortey,
595 1980). It has been proposed that olenid trilobites may have possessed sulfide-oxidising symbionts
596 within their tissues to adapt to benthic conditions prone to episodic anoxia and euxinia (Fortey,
597 2000). Low Pr/Ph ratios together with elevated homohopane indices (%HHI) and
598 dibenzothiophene/phenanthrene ratios (Figure 5) support the notion that oxygen and sulfidic
599 environmental stress was an important factor for marine invertebrates in both the benthic and
600 pelagic realm during the interval associated with the deposition of the Olenidsletta Member,
601 sustained by organic matter remineralisation and consumption of oxidants. Brachiopod
602 assemblages of the Kirtonryggen Formation are low in diversity and dominated by articulated
603 forms (Hansen & Holmer, 2010, 2011). During the deposition of the Olenidsletta Member, a strong
604 diversification in the brachiopods resulted in the dominance of linguliform brachiopods. This
605 diversification and shift in dominance has been interpreted as mainly reflecting the deepening and
606 the changing water column redox conditions during the deposition of the Olenidsletta Member
607 (Hansen & Holmer, 2010, 2011). Overall, productivity constraints from nutrient limitation, as well
608 environmental shifts associated with sea level change and redox-stratification variation would all

609 have contributed to the selection pressure on different marine invertebrate groups and strongly
610 influenced the temporal variability of the marine community structure.

611 While our biomarker assemblages exhibit some of the main characteristic reported
612 previously for Middle-Late Ordovician and Early Silurian sedimentary rocks and oils (e.g., high
613 hopane/sterane ratios, high 3-methylhopane content, C_{29} sterane dominance, and low/absent C_{30}
614 steranes), it extends their temporal range for the first time as valid for marine environments for the
615 Early-Middle Ordovician interval. The combination of biomarker characteristics that we report
616 through the Early-Middle Ordovician are not only unique but fundamentally different than what is
617 observed in younger Paleozoic rocks, as revealed from detailed investigation of Devonian
618 sedimentary organic matter (e.g., Haddad et al., 2016; Martinez et al., 2018). The temporal shifts
619 in marine biomarker assemblages, which is becoming apparent across the breadth of the Paleozoic
620 Era, reflect the irreversible impact that biotic and climatological innovations had on the evolution
621 of life and environment during this extended interval (Lenton et al., 2012).

622

623 **6. Conclusions**

624 Detailed lipid biomarker and stable isotope stratigraphic records were generated for a suite
625 of oil window-mature Early-Middle Ordovician sedimentary carbonates from the eastern terrane
626 of Ny-Friesland, from Spitsbergen, Norway, which were deposited in a paleotropical marine shelf
627 setting. This represents the first time, to our knowledge, that the biomarker and stable carbon and
628 nitrogen isotope systematics have been investigated to better characterise the microbial
629 communities and nutrient cycling for this important time interval of Earth history which witnessed
630 significant climatic and biospheric evolutionary changes. Biomarker assemblage analysis reveals

631 that the organic-lean strata of the Kirtonryggen Formation was deposited in a semi-restricted and
632 shallow oxygenated marine environment with high salinity elevated above typical marine salinity,
633 dominated by bacterial primary producers including likely contributions from benthic microbial
634 mats. The transition from the middle to uppermost Kirtonryggen Formation into the Valhallfonna
635 Formation, around the base of the Olenidsletta Member, represents a local deepening of the basin
636 marked by elevated productivity and deposition of sedimentary rocks with higher organic matter
637 content under a redox-stratified water column, including episodes of photic zone euxinia. The
638 locally nitrate-limiting and oxygen-deficient conditions would have favoured diazotrophs as the
639 dominant primary producers and the low sulfate marine conditions (relative to Mesozoic and
640 younger settings) likely helped sustain active marine methane cycling between the sediment
641 package and the water column. We observed consistently high 3MeHI values mainly in the 5 to
642 15% range (average = 9.9%) which is well above marine Phanerozoic values (typically from 1 to
643 3%) and commonly detected C_{40} acyclic and cyclic biphytane markers derived from archaea.

644 In terms of implications for the enablement and sustenance of the GOBE, sufficient
645 biomass production and replenishment of bioavailable dissolved nitrogen species via nitrogen
646 fixation from diazotrophic bacteria and/or advection of nitrogen or ammonium onto the shelf from
647 exchange with open ocean waters, would have been required to support the heterotrophic nutrient
648 requirements of diverse groups of marine invertebrates. Additionally, the development of water
649 column stratification, with anoxic/euxinic layers shoaling at least episodically into the photic zone,
650 during the deposition of the more organic-rich Olenidsletta Member of the Valhallfonna
651 Formation, shows that changing sea level and redox conditions also influenced the temporal
652 stability of marine invertebrate communities. Olenid trilobite fossils are prominent within this
653 strata and these may have possessed sulfide-oxidising microbial symbionts which helped them

adapt to these metabolically-challenging benthic marine conditions. Distinctive biomarker characteristics reported previously for Middle and Late Ordovician rocks and oils (particularly the exceptionally high 3MeHI values and absence or only traces of 24-npc steranes) are also found here for the first time for the Early-Middle Ordovician from detailed MRM-GC-MS analysis of lipid biomarker assemblages. This emphasises that the Ordovician Period represented an important evolutionary and environmental transition period which led to the reorganisation of the Paleozoic marine biosphere, affecting both microbial and marine invertebrate communities.

7. Acknowledgements

The authors acknowledge Charles Diamond and Aaron Martinez for laboratory assistance and Håvard Kårstad for assistance with field logistics. This work is part of Research in Svalbard (RIS) ID 10467, and was funded by a Packard Foundation grant to SF, a Niarchos Foundation grant to MJH, and a Societas Scientarium Fennica to BK. The authors acknowledge the constructive comments provided by two anonymous reviewers as well as Erdem Idiz, Editor-in-Chief, for handling the manuscript.

8. References

Allmon, W. D., Martin, R. E., 2014. Seafood through time revisited: the Phanerozoic increase in marine trophic resources and its macroevolutionary consequences. *Paleobiology* **40**, 256-287.

673 Alvaro, J. J., Bauluz, B., Subias, I., Pierre, C., Vizcano, D., 2008. Carbon chemostratigraphy of
674 the Cambrian-Ordovician transition in a midlatitude mixed platform, Montagne Noire, France.
675 *Geological Society of America Bulletin* **120**, 962-975.

676 Ambrose, G. J., Kruse, P. D., Putnam, P. E., 2001. Geology and hydrocarbon potential of the
677 southern Georgina Basin, Australia. *The APPEA Journal* **41**(1), 139-163.

678 Azmy, K., Lavoie, D., 2009. High-resolution isotope stratigraphy of the Lower Ordovician St.
679 George Group of western Newfoundland, Canada: Implications for global correlation. *Canadian*
680 *Journal of Earth Sciences* **46**(6), 403-423.

681 Azmy, K., Kendall, B., Brand, U., Stouge, S., Gordon, G. W., 2015. Redox conditions across the
682 Cambrian-Ordovician boundary: Elemental and isotopic signatures retained in the GSSP
683 carbonates. *Paleogeography, Paleoclimatology, Paleoecology* **440**, 440-454.

684 Blumenberg, M., Thiel, V., Riegel, W., Kah, L. C., Reitner, J., 2012. Biomarkers of black shales
685 formed by microbial mats, Late Mesoproterozoic (1.1 Ga) Taoudeni Basin, Mauritania.
686 *Precambrian Research* **196-197**, 113-127.

687 Bottjer, D. J., Ausich, W. I., 1986. Phanerozoic development of tiering in soft substrata suspension-
688 feeding communities. *Paleobiology* **12**(4), 400-420.

689 Brandl, P., 2009. Carbon and oxygen isotopes, stratigraphy, and facies of the Oslobreen Group
690 (northeast Ny Friesland, Svalbard). Diploma thesis, Part B; Geozentrum Nordbayern, Universität
691 Erlangen-Nürnberg, Germany, 114 pp.

692 Brocks, J. J., Love, G. D., Summons, R. E., Knoll, A. H., Logan, G. A., Bowden, S. A., 2005.
693 Biomarker evidence for green and purple sulphur bacteria in a stratified Paleoproterozoic sea.
694 *Nature* **437**(7060), 866-870.

695 Buggisch, W., Keller, M., Lehnert, O., 2003. Carbon isotope record of Late Cambrian to Early
696 Ordovician carbonates of the Argentine Precordillera. *Paleogeography, Paleoclimatology,*
697 *Paleoecology* **195**, 357-373.

698 Cai, C., Li, K., Anlai, M., Zhang, C., Xu, Z., Worden, R. H., Wu, G., Zhang, B., Chen, L., 2009.
699 Distinguishing Cambrian and Upper Ordovician source rocks: Evidence from sulfur isotopes and
700 biomarkers in the Tarim Basin. *Organic Geochemistry* **40**, 755-768.

701 Cao, C., Love, G. D., Hays, L. E., Wang, W., Shen, S., Summons, R. E., 2009. Biogeochemical
702 evidence for euxinic oceans and ecological disturbance presaging the end-Permian mass extinction
703 event. *Earth and Planetary Science Letters* **281**, 188-201.

704 Carrillo-Hernandez, T., Schaeffer, P., Adam, P., Albrecht, P., Derenne, S., Largeau, C., 2003.
705 Remarkably well-preserved archaeal and bacterial membrane lipids in 140 million years old
706 sediment from the Russian platform (Kasphpir oil shales, upper Jurassic). Abstract. 21st
707 International Meeting on Organic Geochemistry, European Association of Organic Geochemists,
708 Krakow, Poland, p. 77-78.

709 Chen, Z., Wang, T-G., Li, M., Yang, F., Chen, B., 2018. Biomarker geochemistry of crude oils
710 and Lower Paleozoic source rocks in the Tarim Basin, western China: An oil-source rock
711 correlation study. *Marine and Petroleum Geology* **96**, 94-112.

712 Collister, J. W., Summons, R. E., Lichtfouse, E., Hayes, J. M., 1992. An isotopic biogeochemical
713 study of the Green River oil shale. *Organic Geochemistry* **19**(1-3), 265-276.

714 Cooper, R. A., Fortey, R. A., 1982. The Ordovician graptolites of Spitsbergen. Bulletin of the
715 British Museum (Natural History), *Geology* **36**, 157-302.

716 Dahl, J., Chen, R. T., Kaplan, I. R., 1989. Alum shale bitumen maturation and migration:
717 Implications for Gotland's oil. *Journal of Petroleum Geology* **12**(4), 465-476.

718 Delabroye, A., Vecoli, M., 2010. The end-Ordovician glaciation and the Hirnantian Stage: A
719 global review and questions about Late Ordovician event stratigraphy. *Earth-Science Reviews*
720 **98**(3-4), 269-282.

721 DeLong, E. F., King, L. L., Massana, R., Cittone, H., Murray, A., Schleper, C., Wakeham, S. G.,
722 1998. Dibiphytanyl ether lipids in nonthermophilic crenarchaeotes. *Applied and Environmental*
723 *Microbiology* **64**(3), 1133-1138.

724 Delwich, C. C., Steyn, P. L., 1970. Nitrogen isotope fractionation in soils and microbial reactions.
725 *Environmental Science & Technology* **4**(11), 929-935.

726 Doughty, D. M., Hunter, R. C., Summons, R. E., Newman, D. K., 2009. 2-Methylhopanoids are
727 maximally produced in akinetes of *Nostoc punctiforme*: geobiological implications. *Geobiology*
728 **7**(5), 524-532.

729 Droser, M. L., Finnegan, S., 2003. The Ordovician Radiation: a follow-up to the Cambrian
730 Explosion? *Integrative and Comparative Biology*, **43**(1), 178-184.

731 Edwards, D. S., Boreham, C. J., Chen, J., Grosjean, E., Mory, A. J., Sohn, J., Zumberge, J. E.,
732 2013. Stable carbon and hydrogen isotopic compositions of Paleozoic marine crude oils from the

733 Canning Basin: Comparisons with other West Australian crude oils. West Australian Basins
734 Symposium, p. 1-32.

735 Edwards, C. T., Saltzman, M. R., 2016. Paired carbon isotopic analysis of Ordovician bulk
736 carbonate ($\delta^{13}C_{carb}$) and organic matter ($\delta^{13}C_{org}$) spanning the Great Ordovician Biodiversification
737 Event. *Paleogeography, Paleoclimatology, Paleoecology* **458**, 102-117.

738 Edwards, C. T., Saltzman, M. R., Royer, D. L., Fike, D. A., 2017. Oxygenation as a driver of the
739 Great Ordovician Biodiversification Event. *Nature Geoscience* **10**, 925-929.

740 Farrell, U. C., Briggs, D. E. G., Gaines, R. R., 2011. Paleoecology of the olenid trilobite Triarthrus:
741 new evidence from Beecher's Trilobite Bed and other sites of pyritization. *Palaios* **26**(11), 730-
742 742.

743 Farrimond, P., Talbot, H. M., Watson, D. F., Schulz, L. K., Wilhelms, A., 2004. Methylhopanoids:
744 molecular indicators of ancient bacteria and a petroleum correlation tool. *Geochimica et*
745 *Cosmochimica* **68**, 3873-3882.

746 Finnegan, S., Bergmann, K., Eiler, J. M., Jones, D. S., Fike, D. A., Eisenman, I., Hughes, N. C.,
747 Tripati, A. K., Fischer, W. W., 2011. The magnitude and duration of the Late Ordovician-Early
748 Silurian glaciation. *Science* **311**(6019), 903-906.

749 Fortey, R. A., 1974. A new pelagic trilobite from the Ordovician of Spitsbergen, Ireland, and Utah.
750 *Palaeontology* **17**(1), 111-124.

751 Fortey, R. A., 1980. The Ordovician trilobites of Spitsbergen: III. Remaining trilobites of the
752 Valhallfonna Formation. *Skrifter Norsk Polarinstitutt* **171**, 1-63.

753 Fortey, R. A., 2000. Olenid trilobites: The oldest known chemoautotrophic symbionts?
754 *Proceedings of the National Academy of Sciences of the United States of America* **97**, 6574-6578.

755 Fortey, R. A., Brunton, D. L., 1973. Cambro-Ordovician rocks adjacent to Hinlopenstretet, north
756 Ny Friesland, Spitsbergen. *Geological Society of America Bulletin* **84**, 2227-2242.

757 Fortey, R. A., Cocks, L. R. M., 2003. Paleontological evidence bearing on global Ordovician-
758 Silurian continental reconstructions. *Earth-Science Reviews* **61**, 245-307.

759 Foster, C. B., Reed, J. D., Wicander, R., 1989. Gloeocapsomorpha prisca Zalessky, 1917: A new
760 study part I: Taxonomy, Geochemistry, and Paleoecology. *Geobios* **22**(6), 735-759.

761 Foster, C. B., Wicander, R., Reed, J. D., 1990. Gloeocapsomorpha prisca Zalessky, 1917: A new
762 study part II: Origin of kukersite, a new interpretation. *Geobios* **23**(2), 133-140.

763 Fowler, M. G., Douglas, A. G., 1984. Distribution and structure of hydrocarbons in four organic-
764 rich Ordovician rocks. *Organic Geochemistry* **6**, 105-114.

765 Fowler, M. G., 1992. The influence of *Gloeocapsomorpha prisca* on the organic geochemistry of
766 oils and organic-rich rocks of Late Ordovician age from Canada. In: Schidlowski, M., Golubic, S.,
767 Kimberley, M., McKirdy, D., Trudinger, P. A. (Eds.), Early Organic Evolution: Implications for
768 Mineral and Energy Resources. Springer-Verlag, Berlin, pp. 336-356.

769 French, K. L., Sepúlveda, J., Trabucho-Alexandre, J., Gröcke, D. R., Summons, R. E., 2014.
770 Organic geochemistry of the early Toarcian oceanic anoxic event in Hawsker Bottoms, Yorkshire,
771 England. *Earth & Planetary Science Letters* **390**, 116-127.

772 French, K. L., Rocher, D., Zumberge, J. E., Summons, R. E., 2015. Assessing the distribution of
773 sedimentary C_{40} carotenoids through time. *Geobiology* **13**, 139-151.

774 Gold, D. A., Grabenstatter, J., de Mendoza, A., Riesgo, A., Ruiz-Trillo, I., Summons, R. E., 2016.
775 Sterol and genomic analyses validate the sponge biomarker hypothesis. *Proceedings of the*
776 *National Academy of Sciences of the United States of America* **113**(10), 2684-2689.

777 Grabenstatter, J., Méhay, S., McIntyre-Wressing, A., Giner, J-L., Edgcomb, V. P., Beaudoin, D.
778 J., Bernhard, J. M., Summons, R. E., 2013. Identification of 24-n-propylidenecholesterol in a
779 member of the Foraminifera. *Organic Geochemistry* **63**, 145-151.

780 Grosjean, E., Love, G. D., Stalvies, C., Fike, D. A., Summons, R. E., 2009. Origin of petroleum in
781 the Neoproterozoic-Cambrian South Oman Salt Basin. *Organic Geochemistry* **40**, 87-110.

782 Guthrie, J. M., and Pratt, L. M., 1995. Geochemical character and origin of oils in Ordovician
783 reservoir rock, Illinois and Indiana, USA. *AAPG Bulletin* **79**, 1631-1649.

784 Haddad, E. E., Tuite, M. L., Martinez, A. M., Williford, K., Boyer, D. L., Droser, M. L., Love, G.
785 D., 2016. Lipid biomarker stratigraphic records through the Late Devonian Frasnian/Famennian
786 boundary: Comparison of high- and low-latitude epicontinental marine settings. *Organic*
787 *Geochemistry* **98**, 38-53.

788 Halverson, G. P., 2011. Glacial sediments and associated strata of the Polarisbreen Group,
789 northeastern Svalbard. In: Arnaud, E., Halverson, G. P., and Shields-Zhou, G. A. (Eds.), The
790 Geological Record of Neoproterozoic Glaciations. Geological Society, London, pp. 571-579.

791 Hansen, J., Holmer, L. E., 2010. Diversity fluctuations and biogeography of the Ordovician
792 brachiopod fauna in Northeastern Spitsbergen. *Bulletin of Geosciences* **85**(3), 497-504.

793 Hansen, J., Holmer, L. E., 2011. Taxonomy and biostratigraphy of Ordovician brachiopods from
794 Northeastern Ny Friesland, Spitsbergen. *Zootaxa* **3076**, 1-122.

795 Hatch, J. R., Jacobsen, S. R., Witzke, B. J., Risatti, J. B., Anders, D. E., Watney, W. L., Newell,
796 K. D., Vuletich, A. K., 1987. Possible Late Middle Ordovician organic carbon isotope excursion:
797 evidence from Ordovician oils and hydrocarbon source rocks, Mid- Continent and east-central
798 United States. *Bulletin of the American Association of Petroleum Geologists* **71**, 1342-1354.

799 Hayes, J. M., Strauss, H., Kaufman, A. J., 1999. The abundance of ^{13}C in marine organic matter
800 and isotopic fractionation in the global biogeochemical cycle of carbon during the past 800 Ma.
801 *Chemical Geology* **161**, 103-125.

802 Jacobsen, S. R., Hatch, J. R., Teerman, S. C., Askin, R. A., 1988. Middle Ordovician organic
803 matter assemblages and their effect on Ordovician-derived oils. *American Association of*
804 *Petroleum Geologists Bulletin* **72**, 1090-1100.

805 Jahren, A. H., Schubert, B. A., Marynowski, L., Wilson, J. P., 2013. The carbon isotope organic
806 geochemistry of Early Ordovician rocks from the Annascaul Formation, County Kerry. *Irish*
807 *Journal of Earth Sciences* **31**, 1-12.

808 Jarrett, A., Edwards, D., Boreham, C., McKirdy, D., 2016. Petroleum geochemistry of the
809 Amadeus Basin. Annual Geoscience Exploration Seminar (AGES) Proceedings, Alice Springs,
810 Nothern Territory, 15-16 March, 2016. Northern Territory Geological Survey Record 2016-001.

811 Kelly, A. E., Love, G. D., Zumberge, J. E., Summons, R. E., 2011. Hydrocarbon biomarkers of
812 Neoproterozoic to Lower Cambrian oils from eastern Siberia. *Organic Geochemistry* **42**, 640-654.

813 Kiipli, E., Kiipli, T., 2013. Nitrogen isotopes in kukersites and black shale implying Ordovician-
814 Silurian seawater redox conditions. *Oil Shale* **30**(1), 60-75.

Kodner, R. B., Pearson, A., Summons, R. E., Knoll, A. H., 2008. Sterols in red and green algae: quantification, phylogeny, and relevance for the interpretation of geologic steranes. *Geobiology* **6**(4), 411-420.

Kröger, B., Servais, T., Zhang, Y., 2009. The origin and initial rise of pelagic cephalopods in the Ordovician. *PLoS One* **4**(9), e7262.

Kröger, B., Desrochers, A., Ernst, A., 2017a. The reengineering of reef habitats during the Great Ordovician Biodiversification Event. *Palaios* **32**(9), 584-599.

Kröger, B., Finnegan, S., Franeck, F., Hopkins, M. J., 2017b. The Ordovician section adjacent to Hinlopenstretet, Ny Friesland, Spitsbergen. *American Museum Novitates* **3882**, 1-28.

Kröger, B., 2018. Changes in the latitudinal diversity gradient during the Great Ordovician Biodiversification Event. *Geology* **46**(2), 127-130.

Kuypers, M. M. M., Blokker, P., Erbacher, J., Kinkel, H., Pancost, R. D., Schouten, S., Sinninghe Damsté, J. S., 2001. Massive expansion of marine archaea during a mid-Cretaceous oceanic anoxic event. *Science* **293**, 92-94.

Kuypers, M. M. M., van Breugel, Y., Schouten, S., Erba, E., Sinninghe Damsté, J. D., 2004. N_2-fixing cyanobacteria supplied nutrient N for Cretaceous oceanic anoxic events. *Geology* **32**, 853-856.

LaPorte, D. F., Holmden, C., Patterson, W. P., Loxton, J. D., Melchin, M. J., Mitchell, C. E., Finney, S. C., Sheets, H. D., 2009. Local and global perspectives on carbon and nitrogen cycling during the Hirnantian glaciation. *Paleogeography, Paleoclimatology, Paleoecology* **276**, 182-195.

Lee, C., Fike, D. A., Love, G. D., Sessions, A. L., Grotzinger, J. P., Summons, R. E., Fischer, W. W., 2013. Carbon isotopes and lipid biomarkers from organic-rich facies of the Shuram Formation, Sultanate of Oman. *Geobiology* **11**(5), 406-419.

Lehnert, O., Stouge, S., Brandl, P. A., 2013. Conodont biostratigraphy in the Early to Middle Ordovician strata of the Oslobreen Group in Ny Friesland, Svalbard. *Zeitschrift der Deutschen Gesellschaft fur Geowissenschaften* **164**, 149-172.

Lenton, T. M., Crouch, M., Johnson, M., Pires, N., Dolan, L., 2012. First plants cooled the Ordovician. *Nature Geoscience* **5**, 86-89.

Li, M., Xiao, Z., Snowdon, L., Lin, R., Wang, P., Hou, D., Zhang, L., Zhang, S., Liang, D., 2000. Migrated hydrocarbons in outcrop samples: Revised petroleum exploration directions in the Tarim Basin. *Organic Geochemistry* **31**(6), 599-603.

Love, G. D., Stalvies, C., Grosjean, E., Meredith, W., Snape, C. E., 2008. Analysis of molecular biomarkers covalently bound within Neoproterozoic sedimentary kerogen. In: Kelley, P. H., Bambach, R. K. (Eds.), From Evolution to Geobiology: Research questions driving paleontology at the start of a new century. Paleontological Society Short Course, Cambridge University Press, Cambridge, pp. 67-83.

Love, G. D., Grosjean, E., Stalvies, C., Fike, D. A., Grotzinger, J. P., Bradley, A. S., Kelly, A. E., Bhatia, M., Bowring, S. A., Condon, D. J., Summons, R. E., 2009. Fossil steroids record the appearance of Demospongiae during the Cryogenian period. *Nature* **457**, 718-722.

Love, G. D., Summons, R. E., 2015. The molecular record of Cryogenian sponges – A response to Antcliffe (2013). *Journal of Paleontology* **58**(6), 1131-1136.

856 Luo, G., Wang, Y., Algeo, T. J., Kump, L. R., Bai, X., Yang, H., Yao, L., Xie, S., 2011. Enhanced
857 nitrogen fixation in the immediate aftermath of the latest Permian marine mass extinction. *Geology*
858 **39**, 647-650.

859 Luo, G., Algeo, T. J., Zhan, R., Yan, D., Huang, J., Liu, J., Xie, S., 2016. Perturbation of the marine
860 nitrogen cycle during the Late Ordovician glaciation and mass extinction. *Paleogeography,*
861 *Paleoclimatology, Paleoecology* **448**, 339-348.

862 Martinez, A. M., Boyer, D. L., Droser, M. L., Barrie, C., Love, G. D., 2018. A stable and
863 productive marine microbial community was sustained through the end-Devonian Hangenberg
864 Crisis within the Cleveland Shale of the Appalachian Basin, United States. *Geobiology*, 1-16.

865 Mastalerz, M., Schimmelmann, A., Hower, J. C., Lis, G., Hatch, J., and Jacobsen, S. R., 2003.
866 Chemical and isotopic properties of kukersites from Iowa and Estonia. *Organic Geochemistry*
867 **34**(10), 1419-1427.

868 Miller, A. I. 1997. Dissecting global diversity patterns: Examples from the Ordovician Radiation.
869 *Annual Review of Ecology and Systematics* **28**, 85-104.

870 Miller, A. I., Mao, S. G., 1995. Association of orogenic activity with the Ordovician Radiation of
871 marine life. *Geology* **23**, 305-308.

872 Miller, A. I., Foote, M., 1996. Calibrating the Ordovician Radiation of marine life: implications
873 for Phanerozoic diversity trends. *Paleobiology* **22**, 304-309.

874 Mustafa, K. A., Sephton, M. A., Watson, J. S., Spathopoulos, F., Krzywiec, P., 2015. Organic
875 geochemical characteristics of black shales across the Ordovician-Silurian boundary in the Holy
876 Cross Mountains, central Poland. *Marine and Petroleum Geology* **66**, 1042-1055.

877 Pancost, R. D., Freeman, K. H., Patzkowsky, M. E., Wavrek, D. A., Collister, J. W., 1998.
878 Molecular indicators of redox and marine photoautotroph composition in the late Middle
879 Ordovician of Iowa, U.S.A. *Organic Geochemistry* **29**(5-7), 1649-1662.

880 Pancost, R. D., Freeman, K. H., Patzkowsky, M. E., 1999. Organic-matter source variation and the
881 expression of a late Middle Ordovician carbon isotope excursion. *Geology* **27**(11), 1015-1018.

882 Pang, H., Chen, J., Pang, X., Liu, L., Liu, K., Xiang, C., 2013. Key factors controlling hydrocarbon
883 accumulations in Ordovician carbonate reservoirs in the Tazhong area, Tarim basin, western
884 China. *Marine and Petroleum Geology* **43**, 88-101.

885 Pawlowska, M. M., Butterfield, N. J., Brocks, J. J., 2013. Lipid taphonomy in the Proterozoic and
886 the effect of microbial mats on biomarker preservation. *Geology* **41**, 103-106.

887 Pehr, K., Love, G. D., Kuznetsov, A., Podkovyrov, V., Junium, C. K., Shumlyanskyy, L., Sokur,
888 T., Bekker, A., 2018. Ediacara biota flourished in oligotrophic and bacterially dominated marine
889 environments across Baltica. *Nature Communications* **9**(1807), 1-10.

890 Peters, K. E., Walters, C. C., Moldowan, J. M., 2005. The Biomarker Guide: Volume 2, biomarkers
891 and isotopes in petroleum systems and Earth history. Cambridge University Press, Cambridge, pp.
892 1132.

893 Rashby, S. E., Sessions, A. L., Summons, R. E., Newman, D. K., 2007. Biosynthesis of 2-
894 methylhopanpolyols by an anoxygenic phototroph. *Proceedings of the National Academy of*
895 *Sciences of the United States of America* **104**(38), 15099-15104.

896 Rasmussen, C. M. Ø., Ullmann, C. V., Jakobsen, K. G., Lindskog, A., Hansen, J., Hansen, T.,
897 Eriksson, M. E., Dronov, A., Frei, R., Korte, C., Nielsen, A. T., Harper, D. A. T., 2016. Onset of

main Phanerozoic marine radiation sparked by emerging Mid Ordovician icehouse. *Scientific Reports* **6**, 18884.

Ricci, J. N., Coleman, M. L., Welander, P. V., Sessions, A. L., Summons, R. E., Spear, J. R., Newman, D. K., 2014. Diverse capacity for 2-methylhopanoid production correlates with a specific ecological niche. *The ISME Journal* **8**, 675-684.

Rohrssen, M., Love, G. D., Fischer, W. W., Finnegan, S., Fike, D. A., 2013. Lipid biomarkers record fundamental changes in the microbial community structure of tropical seas during the Late Ordovician Hirnantian glaciation. *Geology* **41**(2), 127-130.

Rohrssen, M., Gill, B. C., Love, G. D., 2015. Scarcity of the C_{30} sterane biomarker, 24-*n*-propylcholestane, in Lower Paleozoic marine environments. *Organic Geochemistry*, **80**, 1-7.

Rubinstein, C. V., Gerrienne, P., de la Puente, G. S., Astini, R. A., Steemans, P., 2010. Early-Middle Ordovician evidence for land plants in Argentina (eastern Gondwana). *New Phytologist* **188**(2), 365-369.

Ruble, T. E., Bakel, A. J., Philp, R. P., 1994. Compound specific isotopic variability in Uinta Basin native bitumens: paleoenvironmental implications. *Organic Geochemistry* **21**(6-7), 661-671.

Pruss, S. B., Finnegan, S., Fischer, W. W., Knoll, A. H., 2010. Carbonates in skeleton-poor seas: new insights from Cambrian and Ordovician strata of Laurentia. *Palaios* **25**, 73-84.

Saito, R., Kaiho, K., Oba, M., Tong, J., Chen, Z-Q., Tian, L., Takahashi, S., Fujibayashi, M., 2017. Tentative identification of diagenetic products of cyclic biphytanes in sedimentary rocks from the uppermost Permian and Lower Triassic. *Organic Geochemistry* **111**, 144-153.

Saltzman, M. R., Edwards, C. T., Adrain, J. M., Westrop, S. R., 2015. Persistent oceanic anoxia and elevated extinction rates separate the Cambrian and Ordovician radiations. *Geology* **43**, 807-810.

Schwark, L., Empt, P., 2006. Sterane biomarkers as indicators of Paleozoic algal evolution and extinction events. *Palaeogeography, Palaeoclimatology, Palaeoecology* **240**, 225-236.

Schwark, L., Frimmel, A., 2004. Chemostratigraphy of the Posidonia Black Shale, SW Germany II. Assessment of extent and persistence of photic-zone anoxia using aryl isoprenoid distributions. *Chemical Geology* **206**, 231-248.

Schinteie, R., Brocks, J. J., 2017. Paleoecology of Neoproterozoic hypersaline environments: Biomarker evidence for haloarchaea, methanogens, and cyanobacteria. *Geobiology* **15**(5), 641-663.

Scotese, C. R., McKerrow, W. S., 1990. Revised world maps and introduction. *Geological Society, London, Memoirs* **12**, 1-12.

Sepkoski, J. J., Bambach, R. K., Raup, D. M., Valentine, J. W., 1981. Phanerozoic marine diversity and the fossil record. *Nature* **293**, 435-437.

Sepúlveda, J., Wendler, J., Leider, A., Kuss, H-J., Summons, R. E., Hinrichs, K-U., 2009. Molecular isotopic evidence of environmental and ecological changes across the Cenomanian-Turonian boundary in the Levant Platform of Central Jordan. *Organic Geochemistry* **40**, 553-568.

Servais, T., Lehnert, O., Li, J., Mullins, G. L., Munnecke, A., Nützel, A., Vecoli, M., 2008. The Ordovician Biodiversification: revolution in the oceanic trophic chain. *Lethaia* **41**, 99-109.

938 Servais, T., Perrier, V., Danelian, T., Klug, C., Martin, R., Munnecke, A., Nowak, H., Nützel, A.,
939 Vandenbroucke, T. R. A., Williams, M., Rasmussen, C. M. Ø., 2015. The onset of the 'Ordovician
940 Plankton Revolution' in the late Cambrian. *Palaeogeography, Palaeoclimatology, Palaeoecology*
941 **485**, 12-28.

942 Servais, T., Harper, D. A. T., 2018. The Great Ordovician Biodiversification Event (GOBE):
943 definition, concept and duration. *Lethaia* **51**, 151-164.

944 Smolarek, J., Marynowski, L., Trela, W., Kujawski, P., Simoneit, B. T., 2017. Redox conditions
945 and marine microbial community changes during the end-Ordovician mass extinction event.
946 *Global and Planetary Change* **149**, 105-122.

947 Spaak, G., Edwards, D. S., Foster, C. B., Pages, A., Summons, R. E., Sherwood, N., Grice, K.
948 2017. Environmental conditions and microbial community structure during the Great Ordovician
949 Biodiversification Event; a multidisciplinary study from the Canning Basin, Western Australia.
950 *Global and Planetary Change*, **159**, 93-112.

951 Stouge, S., Christiansen, J. L., Holmer, L. E., 2011. Lower Paleozoic stratigraphy of
952 Murchisonfjorden and Sparreneset, Nordauslandet, Svalbard. *Geografiska Annaler (Series A),*
953 *Physical Geography* **93**, 209-226.

954 Strother, P. K., Al-Hajri, S., Traverse, A., 1996. New evidence for land plants from the lower
955 Middle Ordovician of Saudi Arabia. *Geology* **24**(1), 55-58.

956 Summons, R. E., Jahnke, L.L., 1990. Identification of the methylhopanes in sediments and
957 petroleums. *Geochimica et Cosmochimica Acta* **54**, 247-251.

Summons, R. E., Powell, T. G., 1991. Petroleum source rocks of the Amadeus Basin. In: Korsch, R. J., and Kennard, J. M. (Eds.), Geological and geophysical studies in the Amadeus Basin, Central Australia. Bureau of Mineral Resources, Australia, Bulletin v. 236, pp. 511-524.

Summons, R. E., Jahnke, L. J., Hope, J. M., Logan, G. A., 1999. 2-Methylhopanoids as biomarkers for cyanobacterial oxygenic photosynthesis. *Nature* **400**, 554-557.

Sun, Y., Mao, S., Wang, F., Peng, P., Chai, P., 2013. Identification of the Kukersite-type source rocks in the Ordovician stratigraphy from the Tarim Basin, NW China. *Chinese Science Bulletin* **58**(35), 4450-4458.

Tomescu, A. M. F., Pratt, L. M., Rothwell, G. W., Strother, P. K., Nadon, G. C., 2009. Carbon isotopes support the presence of extensive land floras pre-dating the origin of vascular plants. *Paleogeography, Paleoclimatology, Paleoecology* **283**, 46-59.

Trotter, J. A., Williams, I. S., Barnes, C. R., Lécuyer, C., Nicoll, R. S., 2008. Did cooling oceans trigger Ordovician biodiversification? Evidence from conodont thermometry. *Science*, **321**(5888), 550-554.

Trubovitz, S., Stigall, A. L., 2016. Synchronous diversification of Laurentian and Baltic rhynchonelliform brachiopods: Implications for regional versus global triggers of the Great Ordovician Biodiversification Event. *Geology* **44**, 743-746.

Vermeij, G. J., 1995. Economics, volcanos, and Phanerozoic revolutions. *Paleobiology* **21**, 125-152.

Webby, B. D., Droser, M. L., Paris, F., Percival, I., 2004. The Great Ordovician Biodiversification Event, Columbia University Press, New York, p. 484.

Welander, P. V., Coleman, M. L., Sessions, A. L., Summons, R. E., Newman, D. K., 2010. Identification of a methylase required for 2-methylhopanoid production and implication for the interpretation of sedimentary hopanes. *Proceedings of the National Academy of Sciences of the United States of America* **107**, 8537-8542.

Welander, P. V., Summons, R. E., 2012. Discovery, taxonomic distribution, and phenotypic characterisation of a gene required for 3-methylhopanoid production. *Proceedings of the National Academy of Sciences of the United States of America* **107**, 8536-8542.

Xiao, X., Li, M., Huang, S., Wang, T., Zhang, B., Fang, R., Zhang, K., Ni, Z., Zhao, Q., Wang, D., 2016. Source, oil charging history and filling pathways of the Ordovician carbonate reservoir in the Halahatang Oilfield, Tarim Basin, NW China. *Marine and Petroleum Geology* **73**, 59-71.

Zhang, T. G., Shen, Y. A., Algeo, T. J., 2010. High-resolution carbon isotopic records from the Ordovician of South China: links to climatic cooling and the Great Ordovician Biodiversification Event (GOBE). *Paleogeography, Paleoclimatology, Paleoecology* **289**, 102-112.

Zou, C., Qui, Z., Poulton, S. W., Dong, D., Wang, H., Chen, D., Lu, B., Shi, Z., Tao, H., 2018. Ocean euxinia and climate change "double whammy" drove the Late Ordovician mass extinction. *Geology* **46**(6), 535-538.

FIGURE CAPTIONS

Figure 1. A) Map of sampling location in Spitsbergen, Norway. B) Magnified inset of the three sampling sites for the Valhallfonna (PR—Profilbekken Member and PO—Olenidsletta Member) and Kirtonryggen Formations (PS—Spora, Basissletta, and Nordporten Members). C) Paleogeographic distribution of continents during the Early-Middle Ordovician (from Scotese & McKerrow, 1990), star represents low latitude location of Spitsbergen. D) Detailed stratigraphic column of the sampled interval. E) Description of symbols and abbreviations: L—Laurentia; S—Siberia; B—Baltica; and G—Gondwana. Dpg—Dapingian, Olenids.—Olenidsletta, PR—Profilbekken. TR—trilobite, GS—gastropod, CPH—cephalopod, SP—sponge, ECH—echinoderm, art. brachiopod—articulate brachiopod, inart. brachiopod—inarticulate brachiopod.

Figure 2. Thermal maturity profiles through the Kirtonryggen and Valhallfonna Formations. A) Tmax (in °C); B) methylphenanthrene index, MPI; [1.5(3-MP+2-MP)/(P+9-MP+1-MP)]; C) Ts/Ts+Tm; D) C_{29} steranes (C_{29} αααS/(αααS+αααR); E) C_{31} αβ hopanes (C_{31} 22S/C_{31} 22S +22R); and F) C_{30} hopanes (C_{30} βα/C_{30} βα+αβ). Dpg.—Dapingian; Sp.—Spora Member; Olenids.—Olenidsletta Member; PR—Profilbekken Member. Grey dashed bar delineates the Valhallfonna Formation (above) from the Kirtonryggen Formation (below).

Figure 3. Bulk carbon and stable isotopic ratio profiles through the Kirtonryggen and Valhallfonna Formations. A) Carbonate content (in weight percent); B) Total Organic Carbon (TOC, in weight percent); C) Bulk organic carbon isotopes ($\delta^{13}C_{org}$, in ‰ VPDB); and D) bulk nitrogen isotopes ($\delta^{15}N_{total}$, in ‰ vs. air). Dpg.—Dapingian; Sp.—Spora Member; Olenids.—Olenidsletta Member; PR—Profilbekken Member. Grey dashed bar delineates the Valhallfonna Formation (above) from the Kirtonryggen Formation (below).

Figure 4. Selected lipid biomarker ratios through the Kirtonryggen and Valhallfonna Formations. A) Total organic carbon (TOC; in weight percent %); B) Hopane/sterane (sum of C_{27}-C_{35} hopanes/sum of C_{27}-C_{29} diasteranes and regular steranes); C) 2α-methylhopane index, in percent (2MeHI%; C_{31} 2α-methylhopane/2α-methylhopane+C_{30} αβ hopane x 100); D) 3β-methylhopane index, in percent (3MeHI%; C_{31} 3β-methylhopane/3β-methylhopane+C_{30} αβ hopane x 100); E) %steranes for C_{27} (filled circles), C_{28} (grey diamonds), and C_{29} (open squares); F) ratio of paleorenieratane/isorenieratane (paleo/iso) for Valhallfonna Formation samples; and G) Gammacerane index (Gammacerane/C_{30} αβ hopane). Dpg.—Dapingian; Sp.—Spora Member; Olenids.—Olenidsletta Member; PR—Profilbekken Member. Grey shaded bar in B) and D) represent the Phanerozoic marine average; grey dashed bar delineates the Valhallfonna Formation (above) from the Kirtonryggen Formation (below).

Figure 5. Selected lipid biomarker ratios through the Kirtonryggen and Valhallfonna Formations. A) TOC (in weight percent); B) C_{28}/C_{29} steranes; C) C_{29}/C_{30} hopane; D) Pristane (Pr)/Phytane (Ph); E) homohopane index (HHI) in % (C_{35} hopanes/sum of C_{31}-C_{35} homohopanes x 100); F) C_{28} bisnorhopane/C_{30} αβ hopane; and G) dibenzothiophene/phenanthrene (DBT/P). Dpg.—Dapingian; Sp.—Spora Member; Olenids.—Olenidsletta Member; PR—Profilbekken Member. Grey dashed bar delineates the Valhallfonna Formation (above) from the Kirtonryggen Formation (below).

Figure 6. Partial MRM ion chromatograms from the saturated hydrocarbon fraction of PO-92.4 (Olenidsletta Member, Valhallfonna Formation) highlighting the abundance of methylhopanes. A) C_{30} αβ and βα hopanes (white), γ = gammacerane; B) C_{31} 2α-methylhopane (black); C_{31} αβ (S and R) hopanes (light grey); and C_{31} 3β-methylhopane (dark grey); C) C_{31} αβ (S and R) hopanes (light grey); D) C_{32} 2α-methylhopanes (black) and 3β-methylhopanes (dark grey); and E) C_{33} 2α-methylhopanes (black) and 3β-methylhopanes (dark grey).

Figure 7. Partial ion chromatogram acquired in selected ion monitoring (SIM) mode for the aromatic hydrocarbon fraction of a sample from the Profilbekken Member (PR-6) showing A) *m*/*z* 134; open circles denote the C_{13}-C_{22} members of 2,3,6-trimethylated arylisoprenoids, and B) *m*/*z* 546 highlighting C_{40} compounds; p—paleorenieratane and i—isorenieratane.

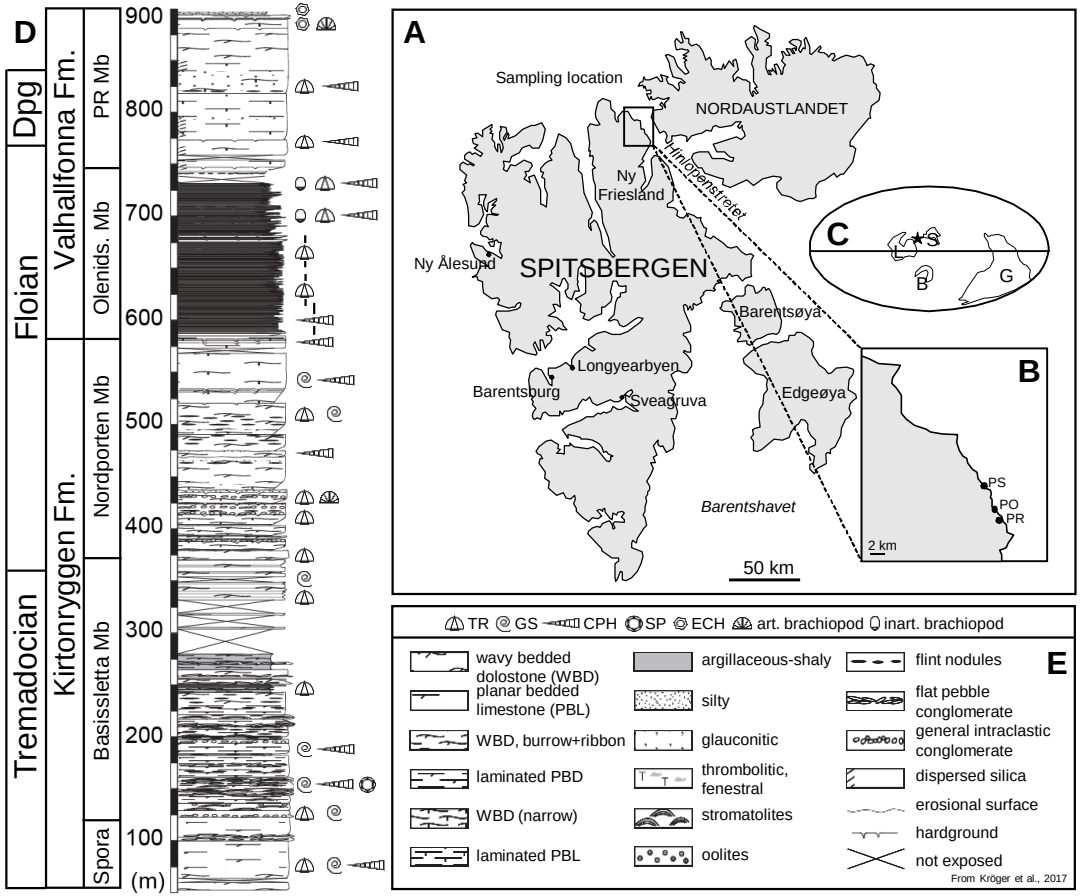
D
Tremadocian
Floian
Dpg
Kirtonryggen Fm.
Valhallfonna Fm.
Spora
Basissletta Mb
Nordporten Mb
Olenids. Mb
PR Mb
900
800
700
600
500
400
300
200
100
(m)
A
Sampling location
NORDAUSTLANDET
Hinlopenstretet
Ny Friesland
Ny Ålesund
SPITSBERGEN
Barentsøya
Longyearbyen
Barentsburg
Sveagruva
Edgeøya
Barentshavet
50 km
C
S
B
G
B
PS
PO
PR
2 km
TR
GS
CPH
SP
ECH
art. brachiopod
inart. brachiopod
wavy bedded dolostone (WBD)
planar bedded limestone (PBL)
WBD, burrow+ribbon
laminated PBD
WBD (narrow)
laminated PBL
argillaceous-shaly
silty
glauconitic
thrombolitic, fenestral
stromatolites
oolites
flint nodules
flat pebble conglomerate
general intraclastic conglomerate
dispersed silica
erosional surface
hardground
not exposed
E
From Kröger et al., 2017

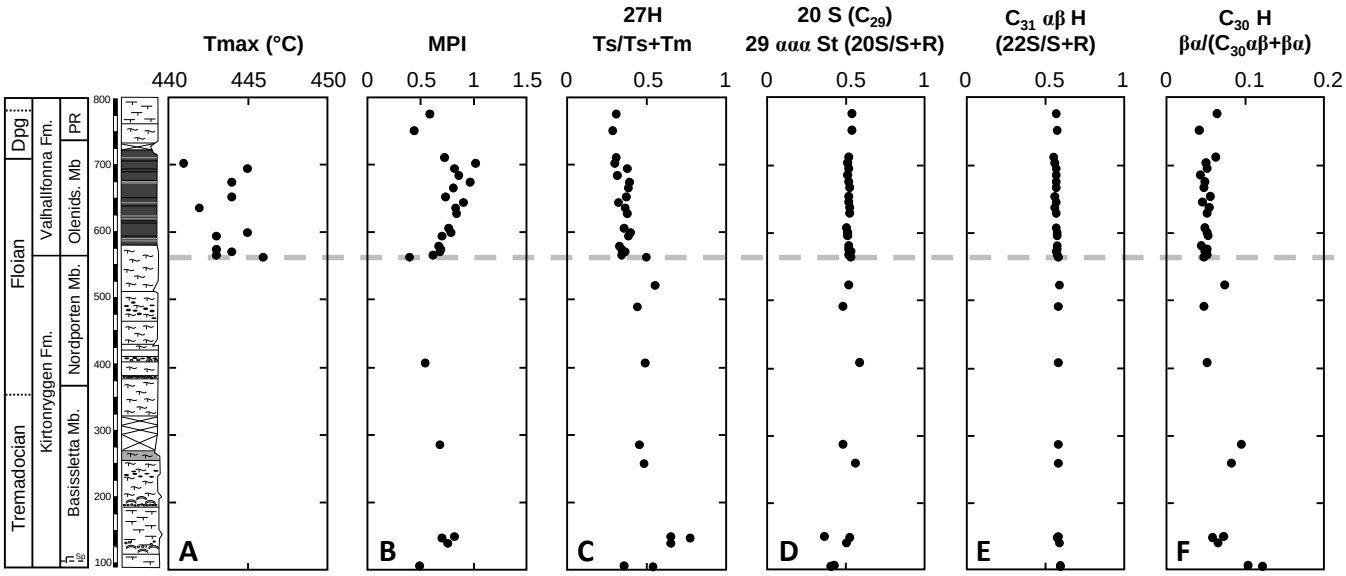
Tmax (°C)
MPI
27H
Ts/Ts+Tm
20 S (C29)
29 ααα St (20S/S+R)
C31 αβ H
(22S/S+R)
C30 H
βα/(C30αβ+βα)
Tremadocian
Floian
Dpg
Kirtonryggen Fm.
Valhallfonna Fm.
Basissletta Mb.
Nordporten Mb.
Olenids. Mb
PR
A
B
C
D
E
F

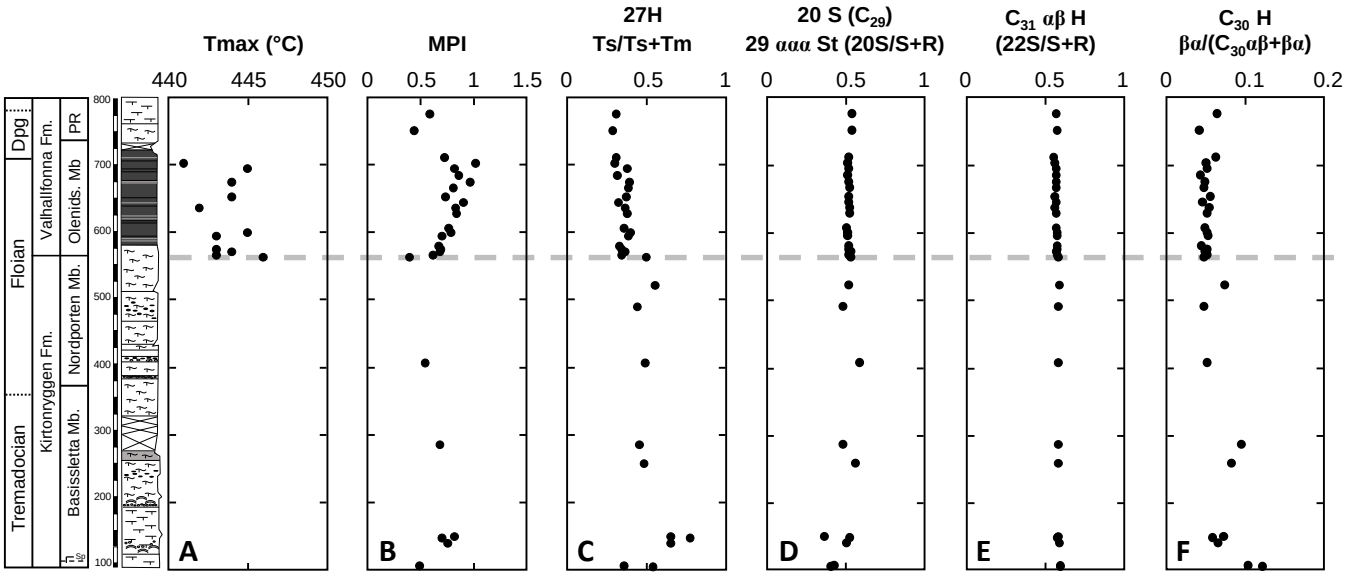
Tmax (°C)
MPI
27H
Ts/Ts+Tm
20 S (C29)
29 ααα St (20S/S+R)
C31 αβ H
(22S/S+R)
C30 H
βα/(C30αβ+βα)
Tremadocian
Floian
Dpg
Kirtonryggen Fm.
Valhallfonna Fm.
Basissletta Mb.
Nordporten Mb.
Olenids. Mb
PR
A
B
C
D
E
F

Tremadocian
Floian
Dpg.
Kirtonryggen Fm.
Valhallfonna Fm.
PR
Olenids. Mb
Nordporten Mb.
Basissletta Mb.
Th
Sp
800
700
600
500
400
300
200
100
TOC wt%
0 2 4 6
A
Hopane/sterane
0 5 10 15
B
2MeHI%
0 5 10 15
C
3MeHI%
0 5 10 15
D
%steranes
10 30 50 70
E
Paleo/Iso
0 1 2 3 4
F
Gammacerane
0 0.5 1
G

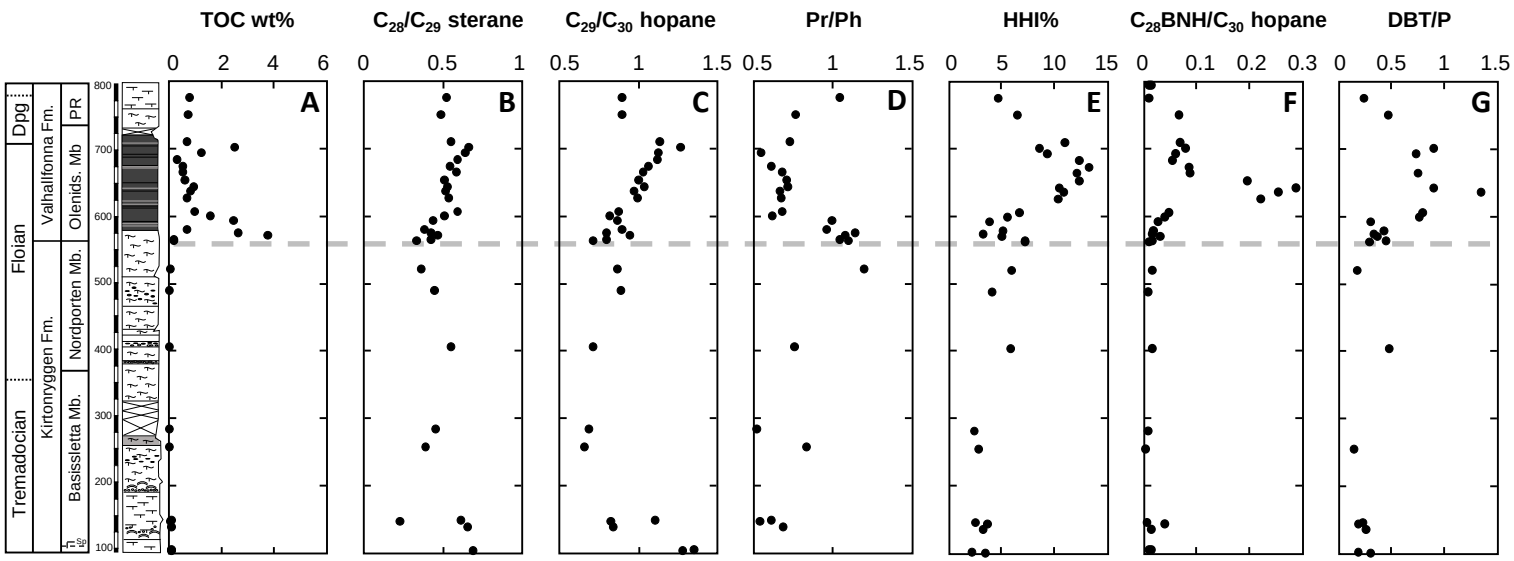
TOC wt%
C28/C29 sterane
C29/C30 hopane
Pr/Ph
HHI%
C28BNH/C30 hopane
DBT/P
A
B
C
D
E
F
G
Tremadocian
Floian
Dpg
Kirtonryggen Fm.
Valhallfonna Fm.
Basissletta Mb.
Nordporten Mb.
Olenids. Mb
PR
Ss

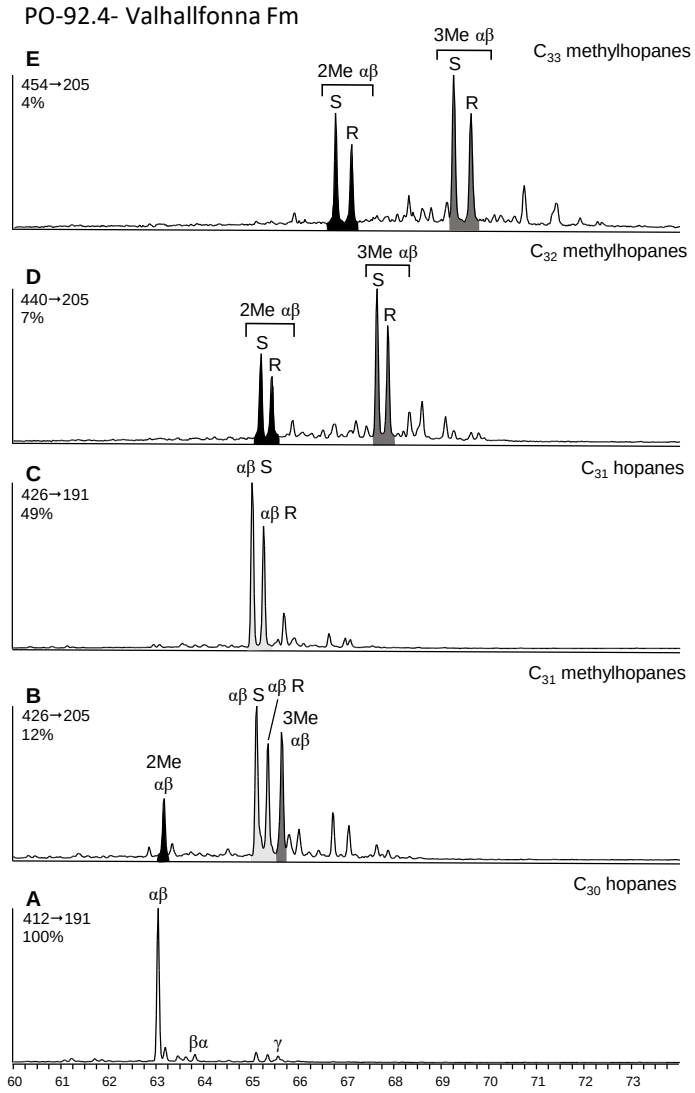
PO-92.4- Valhallfonna Fm
E
454→205
4%
2Me αβ
S
R
3Me αβ
S
R
C33 methylhopanes
D
440→205
7%
2Me αβ
S
R
3Me αβ
S
R
C32 methylhopanes
C
426→191
49%
αβ S
αβ R
C31 hopanes
B
426→205
12%
2Me
αβ
αβ S
αβ R
3Me
αβ
C31 methylhopanes
A
412→191
100%
αβ
βα
γ
C30 hopanes
60
61
62
63
64
65
66
67
68
69
70
71
72
73

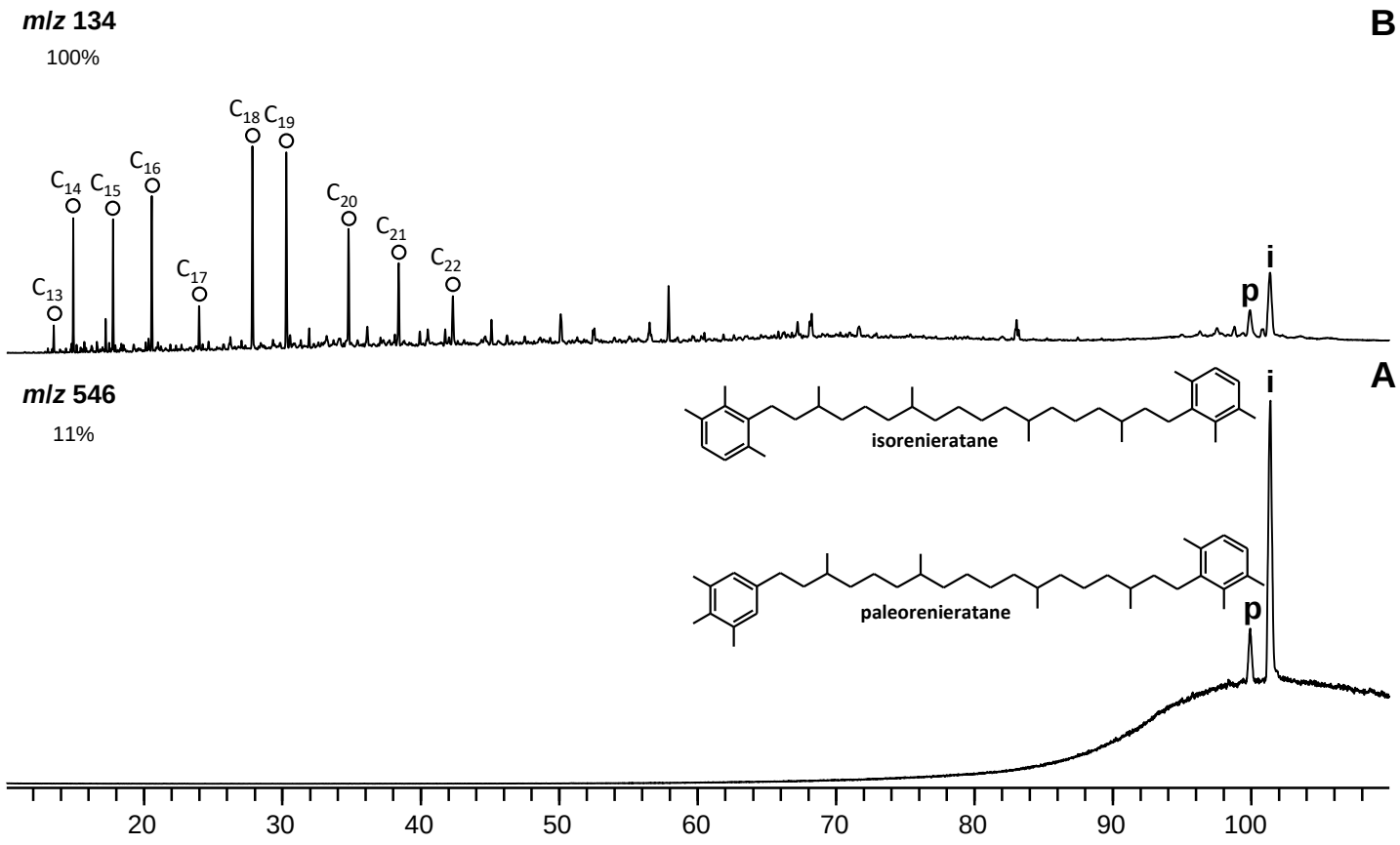
m/z 134
100%
B
C13
C14
C15
C16
C17
C18
C19
C20
C21
C22
p
i
m/z 546
11%
A
isorenieratane
paleorenieratane
p
i
20
30
40
50
60
70
80
90
100